Environment International 172 (2023) 107744

Contents lists available at ScienceDirect

Environment International

journal homepage: www.elsevier.com/locate/envint

Full length article

Phenomenology of ultrafine particle concentrations and size distribution across urban Europe

Pedro Trechera [a,*], Meritxell Garcia-Marlès [a,b,*], Xiansheng Liu [a], Cristina Reche [a], Noemí Pérez [a], Marjan Savadkoohi [a,c], David Beddows [d], Imre Salma [e], Máté Vörösmarty [f], Andrea Casans [g], Juan Andrés Casquero-Vera [g], Christoph Hueglin [h], Nicolas Marchand [i], Benjamin Chazeau [i,j], Grégory Gille [k], Panayiotis Kalkavouras [l,m], Nikos Mihalopoulos [l,m], Jakub Ondracek [n], Nadia Zikova [n], Jarkko V. Niemi [o], Hanna E. Manninen [o], David C. Green [p,q], Anja H. Tremper [p], Michael Norman [r], Stergios Vratolis [s], Konstantinos Eleftheriadis [s], Francisco J. Gómez-Moreno [t], Elisabeth Alonso-Blanco [t], Holger Gerwig [u], Alfred Wiedensohler [v], Kay Weinhold [v], Maik Merkel [v], Susanne Bastian [w], Jean-Eudes Petit [x], Olivier Favez [y], Suzanne Crumeyrolle [z], Nicolas Ferlay [z], Sebastiao Martins Dos Santos [aa], Jean-Philippe Putaud [aa], Hilkka Timonen [bb], Janne Lampilahti [cc], Christof Asbach [dd], Carmen Wolf [dd], Heinz Kaminski [dd], Hicran Altug [ee], Barbara Hoffmann [ee], David Q. Rich [ff], Marco Pandolfi [a], Roy M. Harrison [d,gg], Philip K. Hopke [ff], Tuukka Petäjä [cc], Andrés Alastuey [a], Xavier Querol [a,*]

[a] Institute of Environmental Assessment and Water Research (IDAEA-CSIC), Barcelona, Spain
[b] Department of Applied Physics-Meteorology, University of Barcelona, Barcelona, Spain
[c] Department of Natural Resources & Environment, Industrial & TIC Engineering (EMIT-UPC), Manresa, Spain
[d] Division of Environmental Health and Risk Management, School of Geography, Earth and Environmental Sciences University of Birmingham, Edgbaston, Birmingham, United Kingdom
[e] Institute of Chemistry, Eötvös Loránd University, Budapest, Hungary
[f] Hevesy György Ph.D. School of Chemistry, Eötvös Loránd University, Budapest, Hungary
[g] Andalusian Institute for Earth System Research (IISTA-CEAMA), University of Granada, Granada, Spain
[h] Laboratory for Air Pollution and Environmental Technology, Swiss Federal Laboratories for Materials Science and Technology (Empa), Duebendorf, Switzerland
[i] Aix Marseille Univ., CNRS, LCE, Marseille, France
[j] Laboratory of Atmospheric Chemistry, Paul Scherrer Institute, Villigen, Switzerland
[k] AtmoSud, Regional Network for Air Quality Monitoring of Provence-Alpes-Côte-d'Azur, Marseille, France
[l] Environmental Chemical Processes Laboratory, Department of Chemistry, University of Crete, Heraklion, Greece
[m] Institute for Environmental Research & Sustainable Development, National Observatory of Athens, Athens, Greece
[n] Laboratory of Aerosols Chemistry and Physics, Institute of Chemical Process Fundamentals, Academy of Sciences of the Czech Republic, Rozvojova, Prague, Czech Republic
[o] Helsinki Region Environmental Services Authority (HSY), Helsinki, Finland
[p] MRC Centre for Environment and Health, Environmental Research Group, Imperial College London, UK
[q] NIHR HPRU in Environmental Exposures and Health, Imperial College London, UK
[r] Environment and Health Administration, SLB-analys, Stockholm, Sweden
[s] ENRACT, Institute of Nuclear and Radiological Science & Technology, Energy & Safety, NCSR Demokritos, 1Athens, Greece
[t] Department of Environment, CIEMAT, Madrid, Spain
[u] German Environment Agency (UBA), Dessau-Roßlau, Germany
[v] Leibniz Institute for Tropospheric Research (TROPOS), Leipzig, Germany
[w] Saxon State Office for Environment, Agriculture and Geology (LfULG), Dresden, Germany
[x] Laboratoire des Sciences du Climat et de l'Environnement, CEA/Orme des Merisiers, Gif-sur-Yvette, France
[y] Institut National de l'Environnement Industriel et des Risques (INERIS), Verneuil-en-Halatte, France
[z] University Lille, CNRS, UMR 8518 Laboratoire d'Optique Atmosphérique (LOA), Lille, France
[aa] European Commission, Joint Research Centre (JRC), Ispra, Italy
[bb] Finnish Meteorological Institute, Atmospheric Composition Research, Helsinki, Finland
[cc] Institute for Atmospheric and Earth System Research (INAR), Faculty of Science, University of Helsinki, Finland

* Corresponding authors.
E-mail addresses: pedro.trechera@idaea.csic.es (P. Trechera), meri.garcia@idaea.csic.es (M. Garcia-Marlès), xavier.querol@idaea.csic.es (X. Querol).

https://doi.org/10.1016/j.envint.2023.107744
Received 22 November 2022; Received in revised form 30 December 2022; Accepted 7 January 2023
Available online 13 January 2023

[dd] Air Quality & Sustainable Nanotechnology to Filtration & Aerosol Research, Institute of Energy and Environmental technology e.V. (IUTA), Duisburg, Germany
[ee] Institute for Occupational, Social and Environmental Medicine, Centre for Health and Society, Medical Faculty, University of Düsseldorf, Düsseldorf, Germany
[ff] Department of Public Health Sciences, University of Rochester School of Medicine & Dentistry, Rochester, NY, USA
[gg] Department of Environmental Sciences, Faculty of Meteorology, Environment and Arid Land Agriculture, King Abdulaziz University, Jeddah, Saudi Arabia

ARTICLE INFO

Handling Editor: Olga Kalantzi

Keywords:
Air quality
Aerosols
Atmospheric particulate matter
Nanoparticles
Urban environment
Particle number concentrations

ABSTRACT

The 2017–2019 hourly particle number size distributions (PNSD) from 26 sites in Europe and 1 in the US were evaluated focusing on 16 urban background (UB) and 6 traffic (TR) sites in the framework of **R**esearch **I**nfrastructures services reinforcing air quality monitoring capacities in European **URBAN** & industrial area**S** (RI-URBANS) project. The main objective was to describe the phenomenology of urban ultrafine particles (UFP) in Europe with a significant air quality focus.

The varying lower size detection limits made it difficult to compare PN concentrations (PNC), particularly $PN_{10\text{-}25}$, from different cities. PNCs follow a TR > UB > Suburban (SUB) order. PNC and Black Carbon (BC) progressively increase from Northern Europe to Southern Europe and from Western to Eastern Europe. At the UB sites, typical traffic rush hour PNC peaks are evident, many also showing midday-morning PNC peaks anti-correlated with BC. These peaks result from increased $PN_{10\text{-}25}$, suggesting significant PNC contributions from nucleation, fumigation and shipping.

Site types to be identified by daily and seasonal PNC and BC patterns are: (i) PNC mainly driven by traffic emissions, with marked correlations with BC on different time scales; (ii) marked midday/morning PNC peaks and a seasonal anti-correlation with PNC/BC; (iii) both traffic peaks and midday peaks without marked seasonal patterns. Groups (ii) and (iii) included cities with high insolation.

PNC, especially $PN_{25\text{-}800}$, was positively correlated with BC, NO_2, CO and PM for several sites. The variable correlation of PNSD with different urban pollutants demonstrates that these do not reflect the variability of UFP in urban environments. Specific monitoring of PNSD is needed if nanoparticles and their associated health impacts are to be assessed. Implementation of the CEN-ACTRIS recommendations for PNSD measurements would provide comparable measurements, and measurements of <10 nm PNC are needed for full evaluation of the health effects of this size fraction.

1. Introduction

In spite of the important advances in the science of aerosols and air quality, important scientific and environmental challenges remain unsolved, especially those related to source apportionment of the specific components of atmospheric particulate matter (PM), atmospheric processes influencing aerosols, and the associated climate and health impacts.

One of the issues requiring scientific attention is the origin and variability of ultrafine particles (UFP) (Knibbs et al., 2011; Cassee et al., 2019; Rivas et al., 2021). UFPs have been defined by CEN/TC 264/WG 32 as particles sized <100 nm in diameter ("ISO - ISO/TS 80004-2:2015 - Nanotechnologies — Vocabulary — Part 2: Nano-objects"). PM standards for air quality refer to ambient air mass concentrations below a given aerodynamic diameter per unit volume of air (μg m^{-3}), while UFP concentrations are most commonly (but not exclusively) measured in terms of particle number concentration (PNC) per unit volume of air (particle number or # cm^{-3}). Usually, total PNC is driven by UFP since, in general, >80% of the PNC is accounted for by UFP (Baldauf et al., 2016; Sun et al., 2019). Therefore, in this study we will treat PNC and UFP as synonymous.

It is widely recognised that exposure to PM negatively impacts human health (WHO, 2013, 2021a). In 2016, ambient air pollution accounted for almost seven million premature deaths per year (WHO, 2016), as derived from the aggravation of cardiovascular and respiratory diseases and cancers. Several studies have also shown that UFP can deeply penetrate the respiratory system, thus causing respiratory and cardiovascular diseases in humans (Cassee et al., 2019; Donaldson and Tran, 2002; Kelly and Fussell, 2012; Oberdörster et al., 2005; Salma et al., 2015; Tobías et al., 2018; Valavanidis et al., 2008; Weichenthal et al., 2013). The smaller size of UFPs not only allows them to reach the deeper parts of the respiratory system, but a fraction of these, reaching the alveoli, translocate and reach the circulatory system, and from there can reach any organ in the body (Cassee et al., 2019; Kreyling et al., 2002; Peters et al., 2006, among others). Furthermore, there are evidences that UFP might reach the brain through the olfactory nerve (Maher et al., 2016; Oberdörster et al., 2004).

The new World Health Organisation Air Quality Guidelines (WHO, 2021b) identify UFP concentration as a relevant air quality parameter and find that, although there is a body of evidence for the health effects of UFPs, results are still inconsistent. Cassee et al. (2019) and Rivas et al. (2021) reported that this inconsistency may be, at least in part, due to methodological differences in measurements, to the lack of representation of UFP human exposure to UFPs resulting from the use of only a single monitoring station per city in most studies, and the different sources contributing to UFP concentrations in other cities/regions. Although the WHO (2021b) does not provide guideline values, the monitoring of concentrations of UFPs and black carbon (BC) is recommended to allow a more accurate evaluation of their health effects.

Online measurements of UFP-PNSD (UFP – particle number size distribution) are complex and are usually performed using electrical mobility analysers (Flagan, 1998) in which the particles are charged and separated in sizes by the application of an electrical field, and counted with a condensation particle counter (CPC). This electrical field can be stepped or scanned, allowing sequential measurement of aerosol size distribution. The measurements yield datasets of PNC for multiple-size bins. The particle diameters covered by these systems range from 3 to 16 nm (as lower size detection limits) up to 400 to 1000 nm (as the upper size limit). Since neither total PNC nor UFP-PNSD are included in the current air quality standards, there are no reference methods for these measurements in the context of air quality monitoring. However, CEN has recently developed recommendations for UFP-PNSD measurements from 10 to 800 nm ("CEN/TS 17434:2020 - Ambient air - Determination of the particle number size distribution of atmospheric aerosol using a Mobility Particle Size Spectrometer (MPSS)") and for total PNC measurements ("CEN/TS 16976:2016 - Ambient air - Determination of the particle number concentration of atmospheric aerosol"). Furthermore, ACTRIS (2021) based on Wiedensohler et al. (2012) provide a set of recommendations for the outdoor measurement of both UFP-PNSD and PNC which are close to the CEN standards, but allow for measurement of particles with diameters below 10 nm if required (e.g., Lehtipalo et al., 2022; Manninen et al., 2016).

The lack of harmonisation between these measurements (both in terms of instrumentation and measurement conditions) makes the direct comparison of data from different cities very difficult: a large difference in the lower detection limit might account for a large difference in total PNC or the Nucleation mode (<25 nm). These differences might also lead to inconsistent results when relating UFPs to health effects (Cassee et al., 2019; Rivas et al., 2021). The major differences occur for the PNC of the smaller particle sizes (<25 nm where high PNC and low mass concentrations occur), and may vary over time (i.e., at midday nucleation periods or traffic rush hours) and space (Azimi et al., 2014; Baldauf et al., 2016; Fazli et al., 2019; Gani et al., 2021; Sun et al., 2019; Tobías et al., 2018; Von Bismarck-Osten et al., 2013; Wehner et al., 2002). Thus, primary UFP emitted by traffic are drastically reduced after rush hours, and these are diluted very fast, decreasing concentrations within 10 s of meters from the kerb site (Montagne et al., 2015; Zhu et al., 2002a,b); while secondary UFP might have a smother time and spatial variability (Dall'Osto et al., 2013).

According to a recent review on UFP source apportionment based on UFP-PNSD measurements by Hopke et al. (2022), the typically reported sources of UFP include nucleation, several traffic sources (fresh to aged), domestic and residential heating, regional secondary inorganic aerosols (i.e. regional nitrate and sulphate), particles associated with oxidants as represented by O_3 (i.e. regional secondary organic and inorganic aerosols) and other sources (such as biomass burning, urban background sources, industrial emissions, mixed sources, dust and unknown sources). Shipping and aviation might also contribute to increasing UFP concentrations with a prevalence of the lowest mode (Diesch et al., 2013; Lorentz et al., 2019; Stacey et al., 2021). When focusing on European urban background and traffic sites, traffic UFP contributions dominate PNC, followed by nucleation or new particle formation (NPF), with NPF varying widely according to the climatic region (i.e., it is usually higher in the high-insolation areas; but not consistently) (Bousiotis et al., 2021; Brines et al., 2015; Harrison et al., 2011; Kerminen et al., 2018; Petäjä et al., 2007; Reche et al., 2011; Rivas et al., 2021; Salma et al., 2011; Sun et al., 2019). Focusing on NO_x, several studies agree that one of the main sources of PNC and NO_x are vehicle engines, suggesting that this could be one of the factors behind their strongly correlated (Beevers et al., 2012; Grundström et al., 2015; Johansson et al., 2007). Sánchez Jiménez et al. (2012) corroborated this evidence and also suggest that correlations with NO_x or NO_2 are higher in traffic sites than in urban background sites, because traffic sites are mainly influenced by car emissions and urban background sites may be influenced by common local sources, resulting in a decrease in correlation between PNC and NO_x or PNC and NO_2. In addition, Rivas et al. (2020) also evidenced several sources in the urban background at different European sites where traffic sources were associated with elevated NO_2 concentrations. Wolf et al. (2017) found high levels of correlation between PNC and NO_x concentrations in the city of Augsburg, influenced by common local sources but in this case pointing to traffic and industrial sources as main factors. These studies found that, in urban areas of Europe, the main source contribution arises from road traffic and increases ambient air UFP concentrations with major modes from 15 to 50 nm, depending on the ageing stage (Harrison et al., 2011; Wehner et al., 2002).

Other relevant source contributions include regional UFPs (usually with 80–100 nm modes, Sun et al., 2019) via NPF and growth (e.g., Kerminen et al., 2018). The contribution from NPF is characterised by an increase in UFPs with diameters below 20 nm and has been described as occurring in urban areas in two ways. The first is fast nucleation following the morning UFP peak (caused by high primary semi-volatile exhaust emissions) that nucleates as these dilute and cool (Harrison et al., 2011). The second is the midday or midday-morning UFP peak caused by photochemical NPF occurring with lower levels of pollution (low condensation sink); this may be followed by particle growth, which is attributed to regional (nucleation and growth) or urban (nucleation burst) origins (Hopke et al., 2022; Kerminen et al., 2018; Stanier et al., 2004). UFP concentrations could even be twice as high during NPF events than they are during non-events (e.g., Bousiotis et al., 2021; Casquero-Vera et al., 2021; Németh and Salma, 2014; Thén and Salma, 2022). Recent studies carried out with complex instrumentation to analyse the ion clusters that yield NPF in urban areas found that H_2SO_4 (and probably NH_3 and/or amines) initiate nucleation, while the growth of the nucleated particles is driven by multicomponent condensation of the oxidation products of semi-volatile organic compound (SVOCs) (Bousiotis et al., 2021; Brean et al., 2020; Kulmala et al. 2014; Yao et al., 2018).

RI-URBANS is a European research project (Research Infrastructures Services Reinforcing Air Quality Monitoring Capacities in European Urban & Industrial Areas, the European Union's Horizon 2020 research and innovation program, 101036245) is a European research project which demonstrates the applications of advanced air quality service tools in urban Europe to the assessment of policy decisions in order to better abate pollution and supply accurate information for health studies. The measurement of UFP-PNSD and its applications in air quality assessment is a major goal of RI-URBANS. In this context, this study aims to compile existing UFP-PNSD measurements in urban Europe and to evaluate these data according to (i) the instrumental and methodological approaches implemented; (ii) the comparison of urban concentrations across Europe; (iii) the identification of similarities and major differences; and (iv) the evaluation of relationships with other pollutants, such as BC, PM_x (PM_{10}, $PM_{2.5}$, PM_1), and gaseous pollutants (SO_2, NO, NO_2, O_3, CO), and with meteorological parameters. The results of the source UFP apportionment for the datasets reported here will be presented in a subsequent article.

2. Methodology

2.1. Cities and sites providing UFP-PNSD data

This study is based on UFP-PNSD data from 2017 to 2019 provided by air quality monitoring networks and research supersites to RI-URBANS. These include (Fig. 1 and Table 1):

- Sixteen urban background (UB) sites covering most of Europe: Athens (ATH), Barcelona (BCN), Birmingham (BIR), Budapest (BUD), Dresden (DRE), Granada (GRA), Helsinki (HEL), Langen (LAN), Leipzig (LEI), two in London (LND and LND2), Madrid (MAD), Marseille (MAR), Mülheim (MUL), and Zurich (ZUR), along with and Rochester (ROC) in New York state in the USA.
- Six traffic (TR) sites in Central (C), Western (W) and Northern (N) Europe: DRE, HEL, two in LEI (LEI and LEI2), LND and Stockholm (STO), but none in Southern (S) Europe or Eastern (E) Europe. A TR air quality station BUD providing data on ancillary pollutants is used for interpreting the nearby BUD_UB site, because these pollutants are not measured at BUD_UB.
- Four suburban background (SUB) sites: ATH, Lille (LIL), Paris (PAR) and Prague (PRA).
- One regional background (RB) site in the Po Valley in Italy (Ispra, ISP), which was included because no datasets could be obtained from urban areas in the Po Valley, a pollution hotspot in Europe where most of the PM pollution has a regional origin.

Thus, in total, twenty-seven supersites provided hourly 2017–2019 data on UFP-PNSD for this study. This period was selected to obtain relatively recent data without the effect of the decrease of pollution due to the COVID-19 lockdown-associated measures, which varied both across urban Europe (Eleftheriadis et al., 2021; Putaud et al., 2021; Salma et al., 2020) and globally (Torkmahalleh et al., 2021).

From the twenty-seven sites of the study, twelve have already reported data to the ACTRIS data Centre (EBAS, https://actris.nilu.no/Data/Policy/) (ATH_SUB, GRA_UB, HEL_UB, ISP_RB, MAD_UB, PAR_SUB, PRA_SUB, the three sites from LEI and the two from DRE), but fifteen

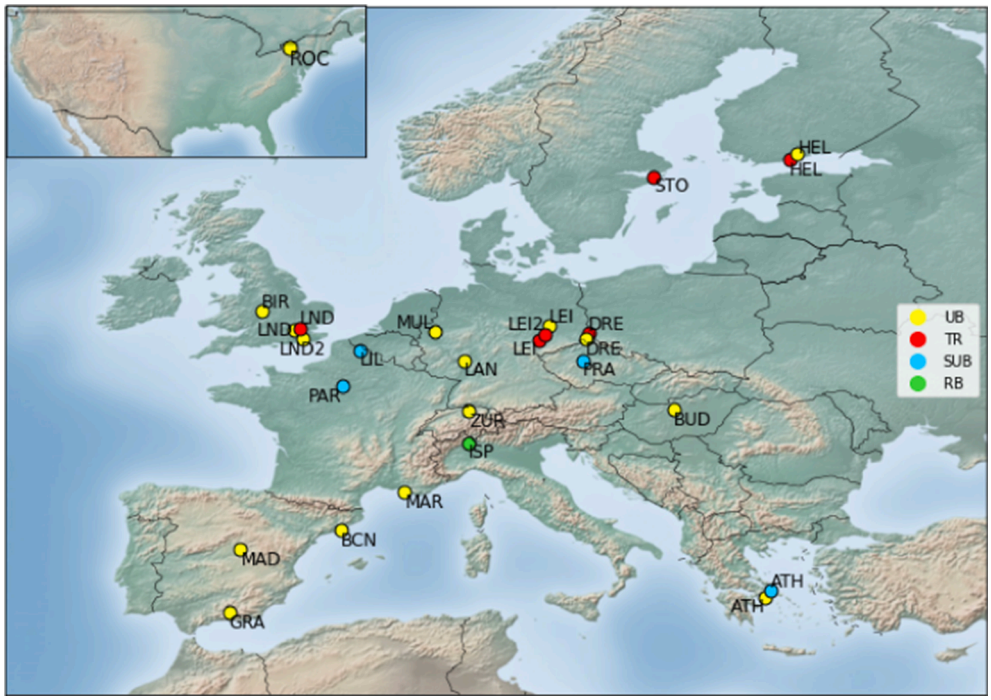

Fig. 1. Location of the cities supplying data on particle number concentrations and size distributions for the present study and the type of station. UB, Urban background; TR, Traffic; SUB, Suburban background; RB, Regional background.

stations have not. Data on co-measured pollutants and meteorological parameters were also collected, when available, from the same sites or nearby air quality monitoring sites.

The selection of cities allowed coverage of the entire European urban concentration ranges of urban pollutants other than UFP (NO, NO_2, BC, PM_x, CO, SO_2 and O_3, Table S1), and of meteorological patterns (Figure S1 and Table S1). The warmest cities were ATH and BCN (with average temperatures of 19 °C), followed by MAD, MAR and GRA (17 °C), BUD, LIL, ISP, ZUR, PAR, MUL, LEI, LAN and BIR (14–12 °C), LND, DRE, ROC, PRA and STO (11–9 °C) and HEL (7 °C). Similarly, a wide range of insolation is also covered, with ATH, MAD, GRA and BCN at an average of 206–187 W m^{-2}, followed by LIL, LAN, ZUR, STO, BUD and ISP (179–150 W m^{-2}) and PAR, HEL, DRE, LEI, BIR and MUL (134–93 W m^{-2}). The most humid cities were BIR, LIL, LND, LAN, PAR, HEL, MUL, PRA, BCN, ISP and DRE (86–70% average relative humidity), followed by STO, LEI, ROC, ZUR and BUD (69–64%) and ATH, MAD and GRA (56–48%). Average wind speed was higher in LND, PRA, STO and MAD (4.3–3.4 m s^{-1}), followed by HEL, MUL, ATH, PAR and BUD (3.3–2.5 m s^{-1}), LAN, ZUR, BCN, LEI, LIL and GRA (2.2–1.4 m s^{-1}) and DRE, MAR and ISP (1.2–0.5 m s^{-1}). However, the different altitudes at which the wind speed was measured in various cities makes it difficult to compare wind speeds appropriately.

2.2. Measurements

The instrumentation used for measuring UFP-PNSD and BC at the different stations is reported in Table 2. Meteorological parameters and concentrations of PM and gaseous pollutants were recorded in each (or nearest) station by instrumentation fulfilling European standards. It is important to note that the gaseous pollutants in Budapest were measured at the nearest station, which is characterised as a typical traffic station (BUD_TR). All the data received were averaged to hourly values.

Different instruments were used to obtain the compiled UFP-PNSD datasets; therefore, the measured size ranges measured varied. The instruments used were the Scanning Mobility Particle Sizer (SMPS), Differential Mobility Particle Sizer (DMPS), Twin Scanning Mobility Particle Sizer (TSMPS) or Twin Differential Mobility Particle Sizer (TDMPS) (Table 2). ACTRIS and CEN guidance (see introduction) recommends a size measurement range of 10–800 nm. However, lower sizes are measured for research purposes (specifically, to study nucleation episodes). Thus, some stations start measuring PNSD at finer sizes (HEL_UB and HEL_TR, 3 and 6 nm, respectively; DRE_TR, 5 nm; BUD_UB, 6 nm) or stop measuring PNSD at coarser upper limits (HEL_UB and TR, 891 nm; BUD_UB, 1000 nm). Nevertheless, the latter affects total PNC to a lower degree than the former because of the relatively low PNC within the coarser sizes. Furthermore, several sites start size measurements at 11 to 17 nm (BCN_UB, BIR_UB, GRA_UB, LIL_SUB, the three sites from LND, MAR_UB, MUL_UB, PAR_SUB, ROC_UB and ZUR_UB) rather than the recommended 10 nm, or stop measurements at lower sizes (410 to 792 nm, the two sites from ATH, BCN_UB, BIR_UB, GRA_UB, LAN_UB, MUL_UB, LIL_SUB, the three sites from LND, MAD_UB, MAR_UB, PAR_SUB, PRA-SUB, ROC_UB, STO_TR and ZUR_UB) than the recommended 800 nm.

2.3. Data treatment

Data treatment and statistical analysis were carried out using R statistical software (v4.1.3) and the *Openair* package (Carslaw and Ropkins, 2012).

3. Results and discussion

3.1. Concentrations of ancillary pollutants

Mean concentrations of NO_2 (Table S2) reached 80 μg m^{-3} in LND_TR and 46 μg m^{-3} in BUD_TR, 30–36 μg m^{-3} in the LEI_TR, STO_TR, GRA_UB, HEL_TR and LND_UB sites, 25–30 μg m^{-3} in the ATH_UB, MAR_UB, DRE_TR, BCN_UB, LND2_UB and LIL_SUB sites, 15–25 μg m^{-3} in the ZUR_UB, LAN_UB, MUL_UB, DRE_UB, BIR_UB, MAD_UB, PRA_SUB and ROC_UB sites, and lower than 15 μg m^{-3} in the ATH_SUB, PAR_SUB, HEL_UB and ISP_RB sites. NO concentrations followed a similar trend with slight differences. Thus, as expected, the highest NO_2 and NO concentrations mainly occurred at the TR > UB > SUB and RB sites, as in

Table 1
List of air quality sites supplying UFP-PNSD datasets to this study with location and type of environment. Coor., Coordinates; Alt., Altitude; UB, Urban Background; TR, Traffic; SUB, Suburban Background; RG, Regional Background.

City (Country)	Station Name	Station type	Acronym	Coor.; (Alt., m a. s.L.)
Athens (GR)	Thissio	UB	ATH_UB	38.00 N, 23.72 E; (110)
Barcelona (ES)	Palau Reial	UB	BCN_UB	41.39 N, 2.13E; (80)
Birmingham (GB)	BAQS	UB	BIR_UB	52.46 N, 1.93 W; (140)
Budapest (HU)	CAAG	UB	BUD_UB	47.48 N, 19.06 E; (115)
Dresden (DE)	Winckelmannstraβe	UB	DRE_UB	51.04 N, 13.73 E; (120)
Granada (ES)	UGR	UB	GRA_UB	31.18 N, 3.58 W; (680)
Helsinki (FI)	SMEARIII	UB	HEL_UB	60.12 N, 24.58 E; (26)
Langen (DE)	UBA	UB	LAN_UB	50.00 N, 8.39 E; (130)
Leipzig (DE)	TROPOS	UB	LEI_UB	51.35 N, 12.43 E; (113)
London (GB)	North Kensington	UB	LND_UB	51.52 N, 0.21 W; (27)
London (GB)	Honor Oak Park	UB	LND2_UB	51.45 N, 0.04 W; (36)
Madrid (ES)	CIEMAT-Moncloa	UB	MAD_UB	40.45 N, 3.73 W; (669)
Marseille (FR)	Longchamp	UB	MAR_UB	43.31 N, 5.39 E; (71)
Mülheim an der Ruhr (DE)	Mülheim-Styrum	UB	MUL_UB	51.45 N, 6.87 E; (39)
Rochester NY (US)	NYS DEC	UB	ROC_UB	43.15 N, 77.55 W; (137)
Zurich (CH)	Kaserne	UB	ZUR_UB	47.38 N, 8.53 E; (410)
Dresden (DE)	North	TR	DRE_TR	51.09 N, 13.76 E; (116)
Helsinki (FI)	Mäkelänkatu Supersite	TR	HEL_TR	60.19 N, 24.95 E: (26)
Leipzig (DE)	Mitte	TR	LEI_TR	51.34 N, 12.38 E; (111)
Leipzig (DE)	Eisenbahnstraβe	TR	LEI2_TR	51.35 N, 12.41 E; (120)
London (GB)	Marylebone Road	TR	LND_TR	51.52 N, 0.15 W; (35)
Stockholm (SE)	Hornsgatan	TR	STO_TR	59.32 N, 18.05 E; (20)
Budapest (HU)	OLM Széna Square	TR	BUD_TR	47.51 N, 19.03 E; (117)
Athens (GR)	Demokritos	SUB	ATH_SU	37.99 N, 23.82 E; (270)
Lille (FR)	Villeneuve d'Ascq	SUB	LIL_SUB	50.61 N, 3.14 E; (70)
Paris (FR)	SIRTA	SUB	PAR_SUB	48.71 N, 2.16 E; (162)
Prague (CZ)	Schudol	SUB	PRA_SUB	50.13 N, 14.38 E; (277)
Ispra (IT)	JRC	RG	ISP_RB	45.80 N, 8.63 E; (209)

urban Europe traffic is the primary source of these pollutants (Nguyen et al., 2018). An increasing concentration trend was also evident from N to S Europe for UB sites, with BIR_UB, ROC_UB and HEL_UB recording the lowest concentrations and cities in E and S Europe the highest, although LND_UB was also among the highest.

Mean concentrations of CO reached the highest value (0.66 mg m^{-3}) in BUD_TR and 0.16 to 0.37 mg m^{-3} at all other sites (excluding the RB) (Table S2). Concentrations of this pollutant were not higher at TR sites compared with UB and SUB sites. Thus, sources beside traffic, such as domestic biomass or coal burning (Querol et al., 2021), were expected. However, problems in measuring this pollutant at low concentrations might also negatively affect comparisons between cities.

Average SO_2 concentrations were <2.2 μg m^{-3} in most cities, except for PRA_SUB, DRE_UB, MAD_UB, BUD_TR, LND_TR, GRA_UB and ATH_UB, where concentrations reached 2.6 to 7.0 μg m^{-3} (Table S2). Higher concentrations are probably associated with the domestic use of coal or oil (EEA, 2021).

Average O_3 concentrations fell in the range of 40–60 μg m^{-3} in most cities except for LND_TR, BUD_TR, MAD_UB, ATH_UB and ATH_SUB with 19, 27, 67, 74 and 82 μg m^{-3}, respectively (Table S2). The traffic sites recorded relatively low concentrations due to the titration of O_3 by NO. Annual urban background O_3 concentrations were higher in HEL (N Europe) than in BCN (S Europe); this was the converse of what was occurring in the background concentrations (EEA, 2021). The higher urban NO concentrations observed over BCN are probably consuming O_3, leading to low O_3 concentrations.

PM_{10} concentrations were markedly higher in the UB sites of BUD, ATH and GRA (33–37 μg m^{-3}), intermediate in ISP_RB and the TR sites of STO, LND, LEI and DRE, PRA_SUB and BCN-UB (20–25 μg m^{-3}), and lower in LIL_SUB, MUL_UB, DRE_UB, HEL_TR, MAR_UB, ATH_SUB, LND2_UB, MAD_UB, ZUR_UB, PAR_SUB, LND_UB, LAN_UB, BIR_UB and HEL_UB (10–19 μg m^{-3}). The highest average $PM_{2.5}$ concentrations were recorded in ATH_UB, BUD_UB and PRA_SUB (16–19 μg m^{-3}), while intermediate (11–15 μg m^{-3}) and lower (4.2–9.2 μg m^{-3}) concentrations were recorded in the same groups of sites listed above for PM_{10}, with slight variations. PM_1 concentrations were measured only in MUL_UB, LND_TR, LND2_UB, LAN_UB, MAR_UB, BCN_UB, LND_UB, BIR_ UB, PAR_SUB and STO_TR (12, 11, 10, 9.1, 8.9, 8.6, 8.0, 7.6, 7.5 and 6.3 μg m^{-3}, respectively). The narrower concentration ranges of PM_1 compared with that of $PM_{2.5}$ probably reflects the higher impact of dust (road dust, desert dust or construction dust) on $PM_{2.5}$ concentrations in the drier MAR and BCN sites compared to the C European cities.

As expected, the twenty-four available datasets of twenty-seven sites indicate that BC concentrations were higher in the TR sites of LND, LEI and LEI2 (1.5–2.7 μg m^{-3}), as well as in the five S European UB sites at GRA, ATH, MAR, BCN and MAD and at ISP_RB (1.2–2.0 μg m^{-3}), and were intermediate in the UK and C European cities (LND2_UB, LIL_SUB, LEI_UB, MUL_UB, LND_UB, BIR_UB, ATH_SUB, DRE_UB and PAR_SUB) and the TR sites of DRE, STO and HEL (0.91–1.1 μg m^{-3}). The lowest concentrations were recorded in the UB sites of ZUR, ROC and HEL (0.33–0.48 μg m^{-3}). BUD, with high levels of traffic-related pollutants,

Table 2
Instruments used to measure UFP-PNSD and BC in the different stations. ND, Not-determined; SMPS, Scanning Mobility Particle Sizer; CPC, Condensation Particle Counter; MAAP, Multi-Angle Absorption Photometer; DMPS, Differential Mobility Particle Sizer; TSMPS, Twin Scanning Mobility Particle Sizer; DMA, Differential Mobility Analyser; TDMPS, Twin Differential Mobility Particle Sizer; UCPC, Ultrafine Condensation Particle Counter; OPC, Optical Particle Counter; UB, Urban Background; TR, Traffic; SUB, Suburban Background; RG, Regional Background.

Station Name	UFP-PNSD Equipment	Range (nm)	BC Equipment
ATH_UB	SMPS TSI 3080L + CPC TSI 3772	10–467	Magee Scientific Aethalometer AE33
BCN_UB	SMPS TSI 3080 + CPC TSI 3772	12–478	THERMO 5012 MAAP
BIR_UB	SMPS TSI 3082 + CPC TSI 3750	13–552	Magee Scientific Aethalometer AE33
BUD_UB	DMPS + CPC TSI 3775	11–816	ND
DRE_UB	TROPOS-TSMPS uses a Vienna-type DMA 28 cm + CPC TSI 3010/3772	10–800	THERMO 5012 MAAP
GRA_UB	SMPS TSI 3082 + CPC TSI 3772	11–496	THERMO 5012 MAAP
HEL_UB	TDMPS Hauke-type DMA 10.9 cm + CPC TSI 3025	10–794	THERMO 5012 MAAP
LAN_UB	SMPS TSI 3080 + TSI 3772, rebuild at TROPOS incl. software	10–544	ND
LEI_UB	TROPOS-TDMPS uses a Vienna-type DMA 11 cm + UCPC TSI 3025	10–800	THERMO 5012 MAAP
LND_UB	SMPS TSI 3080 + CPC TSI 3775 with long DMA	17–604	Magee Scientific Aethalometer AE33
LND2_UB	SMPS TSI 3080 + CPC TSI 3775 with long DMA	17–604	Magee Scientific Aethalometer AE33
MAD_UB	SMPS TSI 3080L + CPC TSI 3775	15–661	Magee Scientific Aethalometer AE33
MAR_UB	SMPS TSI long DMA 3081A + CPC TSI 3752	15–661	Magee Scientific Aethalometer AE33
MUL_UB	SMPS TSI 3080 + CPC TSI 3772	14–496	Magee Scientific Aethalometer AE33
ROC_UB	SMPS TSI 3071 + CPC TSI 3010	11–467	Magee Scientific Aethalometer AE21
ZUR_UB	SMPS TSI 3034 + Nafion aerosol dryer	17–478	Magee Scientific Aethalometer AE33
DRE_TR	TROPOS-SMPS uses a Vienna-type DMA 28 cm + CPC TSI 3772	10–800	THERMO 5012 MAAP
HEL_TR	UHEL DMPS Vienna-type DMA + CPC Airmodus A20	11–800	THERMO 5012 MAAP
LEI_TR	TROPOS-TDMPS uses a Vienna-type DMA 11 cm + UCPC TSI 3025	10–800	THERMO 5012 MAAP
LEI2_TR	TROPOS-TDMPS uses a Vienna-type DMA 11 cm + UCPC TSI 3025	10–800	THERMO 5012 MAAP
LND_TR	SMPS TSI 3080 + CPC TSI 3775 with long DMA	17–604	Magee Scientific Aethalometer AE33
STO_TR	SMPS TSI 3071 + CPC TSI 3775	10–410	Magee Scientific Aethalometer AE33
ATH_SUB	SMPS TSI 3080 + CPC TSI 3772	10–550	Magee Scientific Aethalometer AE33
LIL_SUB	SMPS TSI 3082 + CPC TSI 3750	20–594	Magee Scientific Aethalometer AE33
PAR_SUB	SMPS GRIMM 5416 + OPC GRIMM	11–792	Magee Scientific Aethalometer AE33
PRA_SUB	SMPS TSI 3034 rebuilt at TROPOS	10–519	ND
ISP_RB	DMPS Vienna-type, home-made + CPC TSI 3010/3772	10–800	THERMO 5012 MAAP

did not measure BC.

3.2. Particle number size distributions

The variability of UFP-PNSD concentrations over time is complex due to dynamic processes such as meteorology, emissions and atmospheric processes such as NPF (nucleation), evaporation, condensation, coagulation and deposition (Bousiotis et al., 2021; Harrison et al., 2019; Qi et al., 2015).

As stated in the methodology, comparing concentrations in the compiled PNC datasets was difficult due to the different size detection limits used. Furthermore, in five datasets (BCN_UB, LIL_SUB, MAR_UB, PAR_SUB, ZUR_UB) drastic positive or negative concentrations jumps in the ending lower sizes were detected (Figure S2). This directly affects the UFP PNC and it is for this reason that it has been decided to remove these lower size ranges. This signal is most likely the result of a combination of real concentrations at these sizes and measurement challenges at the low end of size distributions. In the urban environment, size distributions are highly dynamic and variable over a time scale ranging from seconds to minutes. Size distributions are measured by sequentially scanning or stepping through the size range. Close to a source of ultrafine particles, such as in traffic environments, a very localised plume can consequently influence only one or a few size bins. Furthermore, at size ranges close to 10 nm data inversion will amplify small errors due to concurrent low detection efficiency of the CPC and challenges in setting small classification voltages precisely and consistently. This challenge is evident in the study by Wiedensohler et al. (2012) as a higher instrument-to-instrument variability in the size range below 20 nm. The next step to improve the data quality is utilisation of specific instruments for the smaller size ranges (Kangasluoma et al., 2020), which would be operated in parallel with the DMPS/SMPS systems. In this study, to circumvent these challenges for the measurement of UFP-PNSD, the concentration values of the size bins lower than 12 nm in BCN_UB, 20 nm in LIL_SUB, 15 nm in MAR_UB, 11 nm in PAR_SUB and 17 nm in ZUR_UB were deleted (see 'corrected range' in Table S1 and Figure S2). Thus, the minimum detection sizes at all the twenty-seven sites ranged from 3 to 20 nm and the maximum detection sizes ranged from 410 to 1000 nm. The coarser detection size has a small influence on the total PNC. However, the lower size detection limit has a considerable impact, especially on the Nucleation mode ($N_{x\text{-}25}$) concentrations. As an example, HEL_UB measured UFP-PNSD with a size coverage from 3 to 794 nm and Lille from 20 to 594 nm. If we consider the range of 10 to 794 nm or 20 to 794 nm for HEL_UB the total PNC is reduced by 14% or 35% with respect to the 3 to 794 nm measurement. The nucleation mode PNC is reduced by 33% from $N_{3\text{-}25}$ to $N_{10\text{-}25}$ and by 82% from $N_{3\text{-}25}$ to $N_{20\text{-}25}$. However, for HEL_UB, the difference in the PNC from 3–794 nm and 3–594 nm is <0.1%, because the low PNC in the coarse range of the Accumulation mode.

However, only fifteen of the datasets had >70% data availability for the study period and seven even had data availability of <50%. This deficiency reflects the complexity of the UFP-PNSD measurements and the need for detailed supervision and frequent instrumentation maintenance. RI-URBANS strongly recommends not only following the CEN and ACTRIS protocols for measuring PNSD, but also following the guidelines provided by Wiedensohler et al. (2012 and 2018) for the harmonisation of technical standards and data structures to facilitate high quality long-term observations of atmospheric PNSDs and calibration procedures by Wiedensohler et al. (2012 and 2018).

This study analysed the $N_{10\text{-}800}$ and $N_{25\text{-}800}$ concentrations to reduce this effect. In any case, when comparing PNC, one should consider site-specific lower detection sizes. For instance, $N_{20\text{-}594}$ (LIL_SUB) and $N_{10\text{-}800}$ (HEL_UB) were compared as $N_{10\text{-}800}$ = PNC, despite their different sizes.

Once the datasets were corrected and the $N_{10\text{-}800}$ selected, Fig. 2 shows the UFP-PNSD data were classified into the following four groups (as shown Fig. 2):

TR sites (DRE, HEL, LEI, LEI2, STO, LND). These sites have generally high PNCs, with the highest values in the Nucleation mode due to freshly emitted and quickly nucleated particles from traffic exhaust emissions (Harrison et al., 2011; Rönkkö et al., 2017; Sun et al., 2019; Wehner et al., 2002; among others). LND presents low concentrations in the

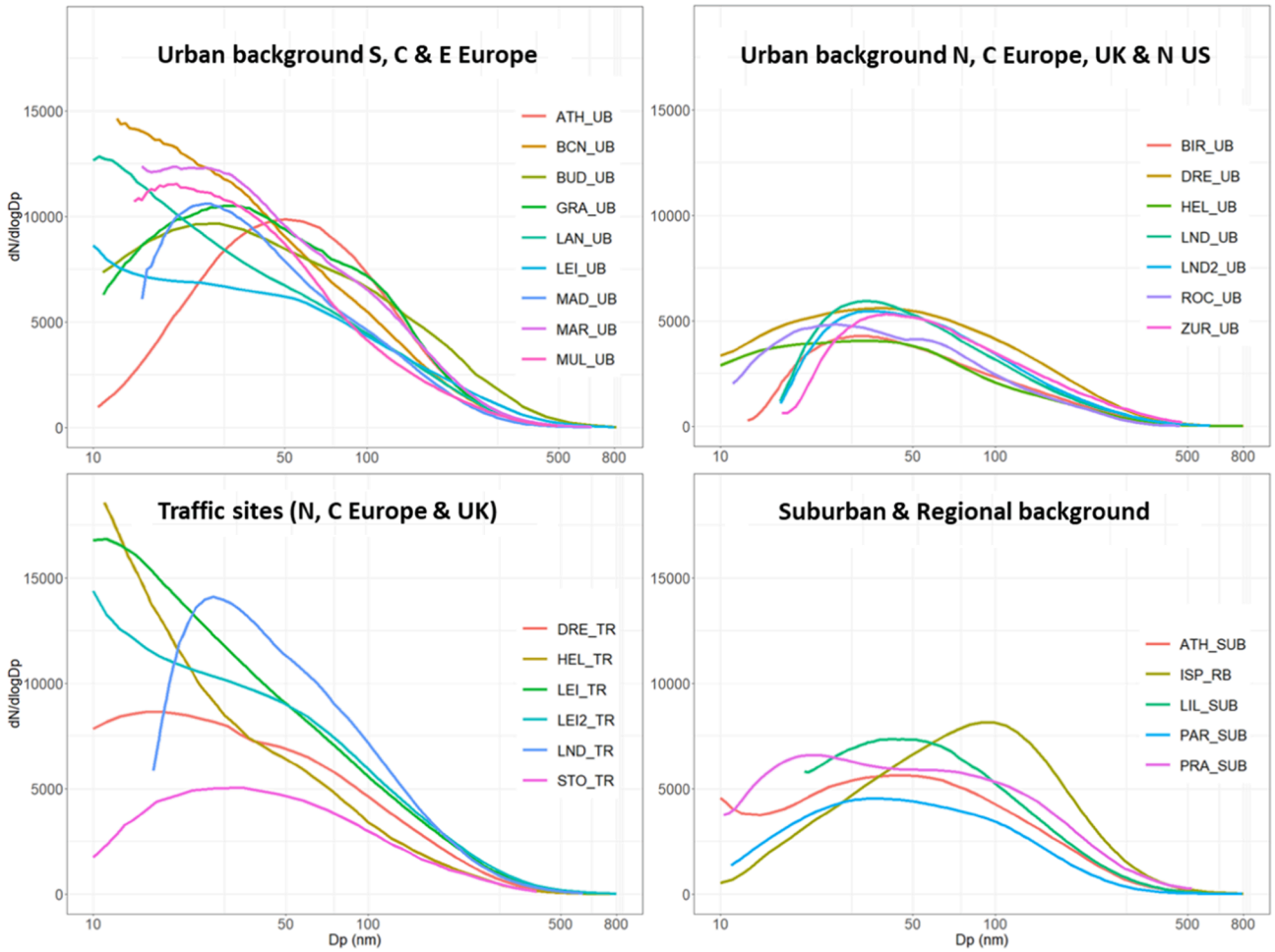

Fig. 2. Averaged 2017–2019 particle number size distributions for Traffic, Urban background sites from S, C and E Europe, Urban background from N, C Europe, UK and N US, and Suburban and Regional background sites.

Nucleation mode and a prominent size mode around 30 nm because the station is in a street canyon with high wind speeds. In this case, particles are being transported and grow due to dynamic processes (Harrison et al., 2019). However, an underestimation of the lowest size fractions cannot be ruled out due to their detection limit (17 nm).

UB sites from S, C and E Europe (ATH, BCN, BUD, GRA, LAN, LEI, MAD, MAR, MUL). Most of these sites also recorded high PNCs, but UFP-PNSDs varied widely. Thus, BCN, MAR, LEI, LAN and MUL are characterised by maxima PNC towards the finer sizes (pointing to a high impact of fresh traffic emissions and NPF). At the same time, ATH had a wide mode at 50 nm (indicating a more aged UFP and/or a relevant regional contribution (Kalkavouras et al., 2021)). The PNSDs at the remaining sites (GRA, BUD and MAD) have an intermediate prevalent mode in the aitken sizes (25–30 nm, indicating an important traffic or airport influence) despite high PNCs in the Nucleation mode.

UB sites from N and C Europe, UK and N US (BIR, DRE, HEL, LND, LND2, ROC, ZUR). These sites recorded relatively low PNCs and a prevalent Aitken mode size (30–40 nm) indicating traffic influence, or possibly airport influence as pointed out by Rivas et al. (2020), with a relatively high load of the Nucleation mode in the cases of DRE, HEL and ROC.

SUB and RB sites (ATH, LIL, PAR, PRA, ISP). These sites recorded PNCs similar to the UB sites in N Europe but with a slightly coarser prevalent mode (50 nm, indicating growth by ageing). As was expected, the PNSD of the RB site (ISP) had a prevalent 100 nm mode, due to the growth processes of the regional UFP in a highly polluted region such as the Po Valley (Sandrini et al., 2014).

3.3. Particle number concentrations

Table 3 summarises the average concentrations of UFP-PNSD, including Nucleation, Aitken and Accumulation modes ($N_{10\text{-}25}$, $N_{25\text{-}100}$ and $N_{100\text{-}800}$, respectively), $N_{25\text{-}800}$ and PNC ($N_{10\text{-}800}$). All concentrations are given in # cm^{-3}.

Focusing on UB sites, the highest PNCs were recorded in BCN, BUD, GRA and MAR (11,200 to 10,300 # cm^{-3}), followed by LAN, MUL, ATH, LEI, MAD and DRE (10,000 to 6200 # cm^{-3}) and LND, LND2, ROC, HEL, ZUR and BIR (4500 to 3500 # cm^{-3}) (Fig. 3). The above concentrations fall in the lower range reported by globally focused studies of UFP. De Jesus et al. (2019) reported a concentration range of 8000 to 19,500 # cm^{-3} for 10 cities located in North America, Europe, Asia, and Australia. The concentration range reported in this present study is similar to that obtained in each of two studies based on data from four European cities (Hofman et al., 2016; Rivas et al., 2020), with 4800–11,300 # cm^{-3}. These values are very close to the < 10,000 # cm^{-3} typical concentrations at urban background concentrations suggested by Cassee et al. (2019). Furthermore, and considering that WHO (2021b) Air Quality Guidelines states that high UFP concentrations can be considered as a health issue if daily averages exceed 10,000 # cm^{-3}, or 20,000 # cm^{-3} on 1-h mean, many of the study sites can be considered as high UFP ones.

TR sites record high PNCs, with 13,500 to 10,500 # cm^{-3} at the LEI, LEI2, LND and HEL sites; followed by 8800 and 5100 # cm^{-3} at DRE and STO (Fig. 3). There are no TR sites supplying UFP-PNSD data in S and E Europe. Kumar et al. (2014) reported differences on into the cities by a factor of 2 to 9 in European cities, with higher concentrations closer to

Table 3
UFP-PNSD arithmetic averages concentrations and their standard deviations, containing Nucleation, Aitken and Accumulation mode ($N_{10\text{-}25}$, $N_{25\text{-}100}$ and $N_{100\text{-}800}$, respectively), $N_{25\text{-}800}$ and PNC ($N_{10\text{-}800}$) from all different stations collected in RI-URBANS. ND, Not-determined; UB, Urban Background; TR, Traffic; SUB, Suburban Background; RG, Regional Background.

Station Name	$N_{10\text{-}25}$ # cm^{-3}	$\sigma_{10\text{-}25}$ # cm^{-3}	$N_{25\text{-}100}$ # cm^{-3}	$\sigma_{25\text{-}100}$ # cm^{-3}	$N_{10\text{-}100}$ # cm^{-3}	$\sigma_{10\text{-}100}$ # cm^{-3}	$N_{100\text{-}800}$ # cm^{-3}	$\sigma_{100\text{-}800}$ # cm^{-3}	$N_{25\text{-}800}$ # cm^{-3}	$\sigma_{25\text{-}800}$ # cm^{-3}	$N_{10\text{-}800}$ # cm^{-3}	$\sigma_{10\text{-}800}$ # cm^{-3}
ATH_UB	1503	1312	5338	4642	6841	5448	1711	2060	7049	6393	8552	7064
BCN_UB	4245	4141	5560	3820	9805	6641	1380	901	6940	4441	11,186	7481
BIR_UB	661	632	2197	1813	2858	2263	673	647	2871	2318	3532	2725
BUD_UB	3691	3075	4973	3333	8664	5785	2173	1465	7146	4408	10,837	6653
DRE_UB	1935	2322	3038	2529	4973	4019	1242	1000	4280	3236	6215	4524
GRA_UB	3129	2677	5629	4160	8758	6230	1776	1431	7406	5395	10,535	7305
HEL_UB	1419	1526	2144	1764	3563	2913	644	507	2789	2056	4208	3119
LAN_UB	4628	4491	4074	2762	8702	5890	1254	888	5328	2999	9956	6657
LEI_UB	3236	4076	3524	2818	6760	5691	1403	1067	4928	3528	8163	6093
LND_UB	614	560	2983	2433	3597	2790	891	1003	3874	3223	4489	3535
LND2_UB	540	405	2912	2256	3452	2509	964	999	3875	3106	4415	3316
MAD_UB	1997	1908	4806	3632	6803	4942	1134	923	5940	4313	7937	5702
MAR_UB	2679	1760	5894	3881	8573	5160	1723	1539	7618	5161	10,297	6274
MUL_UB	2810	2139	5058	3375	7868	4955	1062	804	6120	3855	8930	5351
ROC_UB	1434	1428	2370	1849	3804	2867	602	430	2973	2105	4407	3076
ZUR_UB	296	264	2845	2156	3141	2336	1061	707	3905	2696	4201	2860
DRE_TR	3647	2939	3892	2499	7539	4655	1252	809	5144	3077	8791	5051
HEL_TR	6091	6704	3357	2816	9448	8698	1009	704	4366	3322	10,457	9088
LEI_TR	6711	5725	5272	3062	11,983	7750	1580	936	6852	3696	13,563	8134
LEI2_TR	5249	5252	5075	3368	10,324	7331	1699	1142	6774	4217	12,023	7860
LND_TR	1961	1270	6753	3943	8714	5045	1900	1261	8653	5016	10,614	6070
STO_TR	1646	1441	2756	1807	4402	2848	653	416	3409	2005	5056	3016
ATH_SUB	1654	2749	3245	2469	4899	4561	1203	725	4449	2923	6103	4892
LIL_SUB	560	625	4148	2829	4708	3230	1421	1103	5569	3557	6129	3890
PAR_SUB	1022	1055	2567	1997	3589	2789	876	708	3443	2510	4465	3241
PRA_SUB	2209	2689	3722	2636	5931	4471	1508	1101	5230	3312	7439	4875
ISP_RB	996	1231	4058	2459	5054	2924	2319	2133	6377	4189	7373	4351

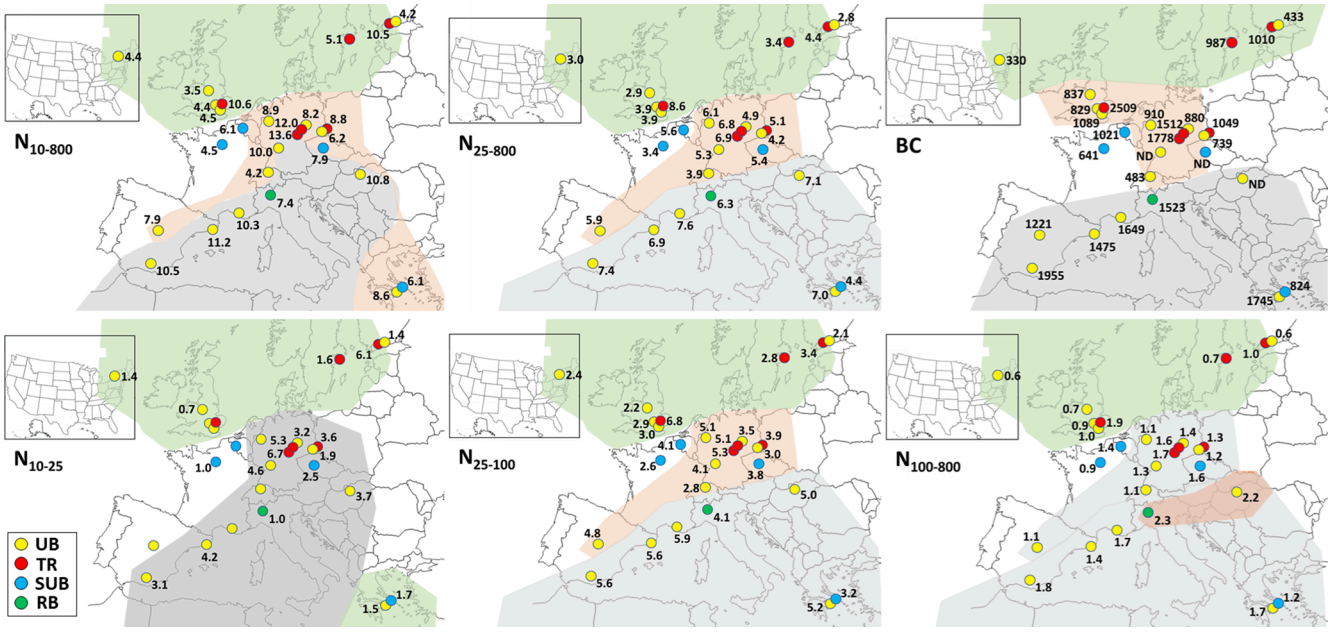

Fig. 3. Regional variability of averaged 2017–2019 particle number concentrations (in # cm^{-3} 10^{-3}) size fractions (in # cm^{-3} 10^{-3}) and black carbon (BC in ng m^{-3}) in Europe. For $N_{10\text{-}25}$, only sites with a lower size detection limit of 10–14 nm are included. UB, Urban background; TR, traffic; SUB, Suburban background; RB, Regional background. Shadowed areas include the UB sites recording the lowest (green), intermediate (orange) and highest (grey) concentrations. (For interpretation of the references to colour in this figure legend, the reader is referred to the web version of this article.)

the traffic sites, however in this study this factor is considerably lower (1.2 to 2.5). Moreover, Morelli et al. (2015), Sánchez Jiménez et al. (2012) and Sun et al. (2019) reported the high PNC concentrations for TR sites from 5 European countries, with values of 11,100 to 25,000 # cm^{-3}.

Additionally, the SUB and RB sites recorded relatively low concentrations, with 7400 to 4500 # cm^{-3} in PRA_SUB, ISP_RB, LIL_SUB, ATH_SUB and PAR_SUB (Fig. 3). Vratolis et al. (2019) reported a mean value of 7600 # cm^{-3} in the size range 13 to 661 nm for the period June to August 2012 at the ATH_SUB station. The results thus show, in addition to the higher TR UFP concentrations generally reported by other studies, such as Sánchez Jiménez et al. (2012), Sun et al. (2019), Thén and Salma (2022), among others, a clear increasing trend of UB PNC from N (3500–4500 # cm^{-3}) to C (6200–10,000 # cm^{-3}) to S

(10,300–11,200 # cm^{-3}) Europe (Fig. 3); this is probably associated with higher pollution levels, insolation (and NPF) and the impact of shipping emissions. This European spatial pattern is quite similar to that found for O_3 (EEA, 2021), although no correlation has been found between O_3 and PNCs in the present study. The increase in both PNCs and O_3 is most likely favoured by atmospheric conditions and emission patterns in S and E Europe (Carnerero et al., 2019).

When the $N_{25\text{-}800}$ values were compared to UFP concentrations (Fig. 3) without the artefact of the different lower size detection limit, a similar (to PNC) N-C-S Europe increasing trend and higher TR-UFP concentrations were again observed. Thus, TR sites reached 4400 to 8700 # cm^{-3} $N_{25\text{-}800}$, except for STO_TR (3400 # cm^{-3}). For UB sites, the highest concentrations were reached in S and E European sites (5900–7600 # cm^{-3}), intermediate concentrations in C European sites (3900–6200 # cm^{-3}), and the lowest concentrations in N European sites, including the UK and ROC (2800–3900 # cm^{-3}). The main difference found between the spatial pattern of $N_{25\text{-}800}$ and that of $N_{10\text{-}800}$ was the inclusion of ATH_UB in the S European high concentration range of $N_{25\text{-}800}$, but in the intermediate range of $N_{10\text{-}800}$, which indicates the low relevance of NPF processes in ATH compared to cities in the W Mediterranean.

Alternatively, the preservation of the N-C-S Europe increasing N-C-S Europe UFP trend when evaluating $N_{25\text{-}800}$ points to higher pollution over S and E Europe as the primary cause of this spatial trend, to a greater degree than higher NPF associated with meteorological characteristics. This finding is also supported by the spatial patterns of concentrations of BC (Fig. 3), which are very close to those of $N_{25\text{-}800}$. First, the TR sites reached the highest BC (0.99–2.7 μg m^{-3}), with the highest concentrations in LND (again, the reader might consider that TR sites from S and E Europe were not included in this study). For the UB sites, the highest BC concentrations were reached again reached in S Europe (1.2 and 2.0 μg m^{-3}), the intermediate concentrations (0.74–1.1 μg m^{-3}) in C Europe and the UK, excluding ZUR (0.48 μg m^{-3}), and the lowest concentrations (0.32–0.43 μg m^{-3}) in N Europe and ROC in N US. The main difference in the spatial patterns of UB sites in Europe is the inclusion of the UK sites in the intermediate concentration range (comparable to C Europe) for BC and the low range (comparable to N Europe) for $N_{25\text{-}800}$. According to prior studies (i.e., Reche et al., 2011), the main source of BC in urban areas of European cities is road traffic (especially pre-Euro5 diesel vehicles), however the contribution of other sources such as biomass or agricultural burning cannot be excluded. The typical diurnal patterns of BC associated with hourly traffic (see below) in these cities points to road traffic as the major source.

3.4. Particle number concentrations according to size

The aforementioned differences in lower size detection limits and the correction of diffusion losses for the datasets compiled in this study was a significant drawback when comparing $N_{10\text{-}25}$. Thus, independently of the location and type of site, for those starting measurements at 10–14 nm the Nucleation mode reached 34 ± 11% of PNC, while for those starting at 15–20 nm it reached only 16 ± 7%. Therefore, the proportions of the Nucleation/Aitken/Accumulation modes in PNC are only discussed for those distributions starting at 10–14 nm. For this subset of sites, the highest Nucleation mode proportions in PNC were reached at the TR sites (42–58%, excluding STO, 33%). For UB sites, the lowest proportions were reached in ATH and BIR (18 and 19%, respectively), intermediate proportions (30–34%) in GRA, BUD, MUL, HEL and DRE, and the highest proportions (38–46%) in BCN, LEI and LAN. Consequently, for the UB: (i) the highest proportion of Nucleation mode concentrations was reached not only at sites from S Europe, but especially in C Europe (LEI and LAN), followed by one site in S Europe (BCN); and (ii) one S Europe site (ATH) had the lowest proportions due to the high concentration sink in this urban zone, which produced high concentrations of Aitken and Accumulation modes (Vratolis et al., 2019). In addition, moderately low Nucleation mode proportions were found at the SUB sites of PRA, ATH and PAR (32, 27 and 23%), with the lowest at ISP_RB (14%). Accumulation mode proportions for PNC reached only 10–20% in all evaluated datasets, excluding ISP_RB at 31%. Aitken mode proportions reached 32–44% of PNC at the TR sites, excluding STO at 54%; 41–57% at the UB sites (with the highest at BIR and ATH, both 62%); and 48–57% at all SUB and RB sites.

The percentage of UFP ($N_{10\text{-}100}$) in PNC reached an average of 84 ± 3.7% for all TR, UB and SUB sites with measurements starting at sizes ranging from 10–14 nm, and 69% in the RB. The data cannot resolve the contribution of sub-10 nm aerosols. Consequently, processes such as formation of newly formed particles by nucleation occur below the detection limit (Okuljar et al. 2021; Rönkkö et al. 2017).

The higher Nucleation mode proportions for PNC in specific UB sites of C Europe (LAN and LEI), with lower insolation than in S Europe, suggest that photochemical regional or urban NPF did not exclusively drive the high proportions of the Nucleation mode, as previous work has concluded (Dall'Osto et al., 2013), but is also influenced by traffic contributions (Bousiotis et al., 2021: Harrison et al., 2011; Sun et al., 2019; Wehner et al., 2002) and the fumigation of the surface by higher-altitude atmospheric layers enriched in $N_{10\text{-}25}$ by NPF processes during the growth of the planetary boundary layer (PBL) (Junkermann et al., 2016); the impact of airports (Rivas et al., 2019), shipping, power plants or industrial pollution plumes might also play a significant role (Cheung et al., 2011; Diesch et al., 2013; Junkermann et al., 2016; Petzold et al., 2008; Stacey et al., 2021; Thomson et al., 2018). A relevant contribution to PNC from regional transport of UFP and the inhibition of relevant NPF might be major causes of the lowest proportion of Nucleation mode particles in ATH and coarser UFP compared with other UB sites (Kalkavouras et al., 2021).

3.4.1. Nucleation mode ($N_{10\text{-}25}$)

Considering only those sites with <14 nm as lower size limit for the PNSD measurements, the absolute Nucleation mode concentrations were lower at the SUB (1000–2200 # cm^{-3}) and RB (1000 # cm^{-3}) sites and markedly higher at the UB (1500–4600 # cm^{-3}, excluding BIR_UB, with 700 # cm^{-3}) and TR sites (3600–6700 # cm^{-3}, excluding STO_TR, with 1600 # cm^{-3}). Considering only UB sites, $N_{10\text{-}25}$ were higher in C, E and SW Europe (2800–4600 # cm^{-3}, excluding DRE, 1900 # cm^{-3}) and lower in N and SE Europe and N US (700–1500 # cm^{-3}). The highest UB Nucleation mode concentrations were recorded at the following sites in the order: LAN > BCN > BUD > LEI > GRA > MUL > DRE > ATH > ROC > HEL. Therefore, as previously stated, it is not the case that S Europe (with higher insolation) records the highest concentrations of the Nucleation mode, but the contribution of other sources and processes (see above) probably significantly contributes to increasing the finest UFPs, especially in C and E Europe.

3.4.2. Aitken mode ($N_{25\text{-}100}$)

For the Aitken mode, all twenty-seven datasets were considered since all sites started measurement at lower sizes than 25 nm. Small differences were found between the Aitken mode concentrations obtained at TR sites (2800–6800 # cm^{-3}) and those obtained at UB (2100–5900 # cm^{-3}), SUB (2600–4100 # cm^{-3}) and RB (4100 # cm^{-3}) sites. However, in the last case, the reader must consider that ISP is located in the Po Valley. The lack of data from TR sites in S Europe makes it difficult to compare concentrations at TR versus UB sites across Europe. However, for UB sites, marked regional trends were again found, with the highest concentrations in S Europe (4800–5900 # cm^{-3}), intermediate concentrations in C Europe (2800–5100 # cm^{-3}) and the lowest concentrations in N Europe, the UK and N US (2100–3000# cm^{-3}); again, this runs parallel to the air pollution trends.

3.4.3. Accumulation mode ($N_{100\text{-}800}$)

The Accumulation mode concentrations at the UB sites were also higher in S Europe (1400–2200 # cm^{-3}, excluding MAD, 1100 # cm^{-3}) than in C (1100–1400 # cm^{-3}) and N Europe, the UK and N US

(600–1000 # cm^{-3}). Variability was high at the SUB and RB sites, with three SUB sites in the range 1200–1500 # cm^{-3}, PAR_SUB at 900 # cm^{-3} and ISP_RB at 2300 # cm^{-3}. Because the coarser detection limit varies across these datasets from 400 to 800 nm, it is difficult to make robust conclusions for this size mode.

3.5. Time variability, daily and seasonal patterns of PNC and BC

BC and PNC concentrations have parallel daily patterns, with the highest concentrations found during traffic rush hours at most sites (Fig. 4), as observed in many prior studies (Joerger and Pryor, 2018; Rivas et al., 2020; Sun et al., 2019; Von Bismarck-Osten et al., 2013;). Furthermore, a considerable number of these (LEI_UB, BCN_UB, LEI_TR and LEI2_TR, LAN_UB, MUL_UB, DRE_TR, BUD_UB, GRA_UB, ATH_UB, ATH_SUB, PRA_SUB and DRE_UB) recorded late morning-midday PNC peaks with very low BC (Fig. 4). In these cases, the intensity of the PNC midday peak varied widely, from those sites where similar concentrations to those found in the traffic rush hour peak were reached (the three LEI sites, BCN_UB, ATH_SUB, MUL_UB, the two DRE sites, BUD_UB and LAN_UB) to others where the midday peak was markedly lower than concentrations from traffic (ATH_UB, GRA_UB and PRA_SUB). Fig. 5 reveals that Nucleation mode peak concentrations, mainly caused by this midday PNC increase, were higher than those recorded during traffic rush hours for a considerable proportion of the sites (see the three LEI sites, BCN_UB, LAN_UB, MUL_UB, the two DRE sites, ATH_UB, ATH_SUB, PRA_SUB and ISP_RB). In these cases, the aforementioned photochemical nucleation and the fumigation of higher-altitude air layers rich in Nucleation mode particles, along with pollution plume impacts, made relevant contributions to PNC, and especially to $N_{10\text{-}25}$.

When simultaneously evaluating daily and seasonal patterns of PNC and BC, the following three types of sites were considered:

Road traffic controlling ambient PNC ($N_{10\text{-}800}$): This type of site, of which ATH_UB is an example (see bottom of Fig. 6), had a PNC peak at traffic rush hours and a PNC which was co-variant with BC (and NO_2, NO, NO_x and CO, not shown). Furthermore, the seasonal trends of BC and PNC were very similar, with high winter and low summer concentrations. At these sites, the midday PNC peak was very weak (or absent) compared with peaks during traffic rush hours. Thus, the daily BC and PNC trends were also very similar. In this case, the highest (but still very soft) midday Nucleation mode occurred in winter-autumn, not in summer as in most cases. Furthermore, these sites were characterised by markedly lower weekend concentrations of both BC and PNC, pointing to a high impact of traffic emissions on the concentrations of both variables. The study sites with similar behaviour are GRA_UB, HEL_TR, MAD_UB, MAR_UB, PAR_SUB, ROC_UB, STO_TR and ZUR_UB (Table S3).

Conversely, some sites had **higher midday/morning PNC, than traffic rush hour:** An example is LEI_UB (see top of Fig. 6), in which the highest PNC was recorded outside traffic rush hours, at around 11–12 h. Hourly variations of averaged PNC were in parallel with O_3 (both maximising at midday) and anti-correlated with BC (PNC maximising at midday and BC being the lowest at midday and the highest at traffic rush hours). The midday PNC peak occurred (in summer, and also in spring and autumn with lower intensity) with very low BC concentrations. This can be attributed to regional or urban photo-nucleation and fumigation from higher atmospheric layers (enriched in Nucleation mode UFP and O_3 and depleted in BC, as the PBL grows by convective dynamics), and/or shipping and aviation and/or power plants and industry (see references above). In these cases, PNC maximised in summer and BC exhibited an opposite seasonal trend, with higher winter values. In most cases, weekend BC and UFP concentrations were lower. Sites included in this type are LEI_TR, LEI2_TR, DRE_UB, LAN_UB and PRA_SUB (Table S3).

Intermediate type sites (different degrees of the prevalence of traffic/midday peaks and weak seasonal patterns): An example is BCN_UB (see middle of Fig. 6). At this site, both traffic and midday peaks were present. Thus, PNC was parallel with BC except during the midday

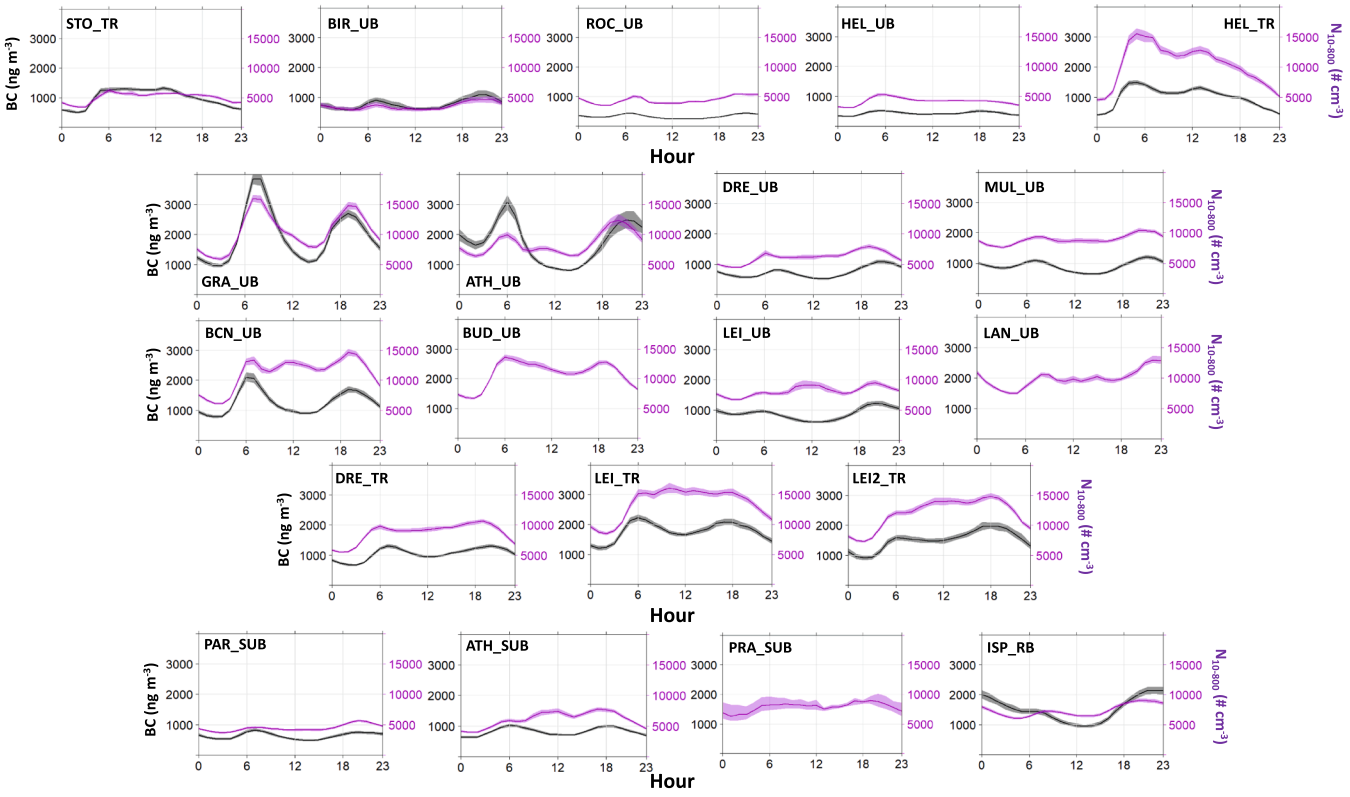

Fig. 4. Averaged 2017–2019 hourly concentrations of the particle number $N_{10\text{-}800}$ and black carbon (BC). Only sites with a lower size detection limit of 10–14 nm are included are considered. UB, Urban background; TR, Traffic; SUB, Suburban background; RB, Regional background. Particle number concentration units are # cm^{-3} 10^{-3} and those of BC in μg m^{-3}.

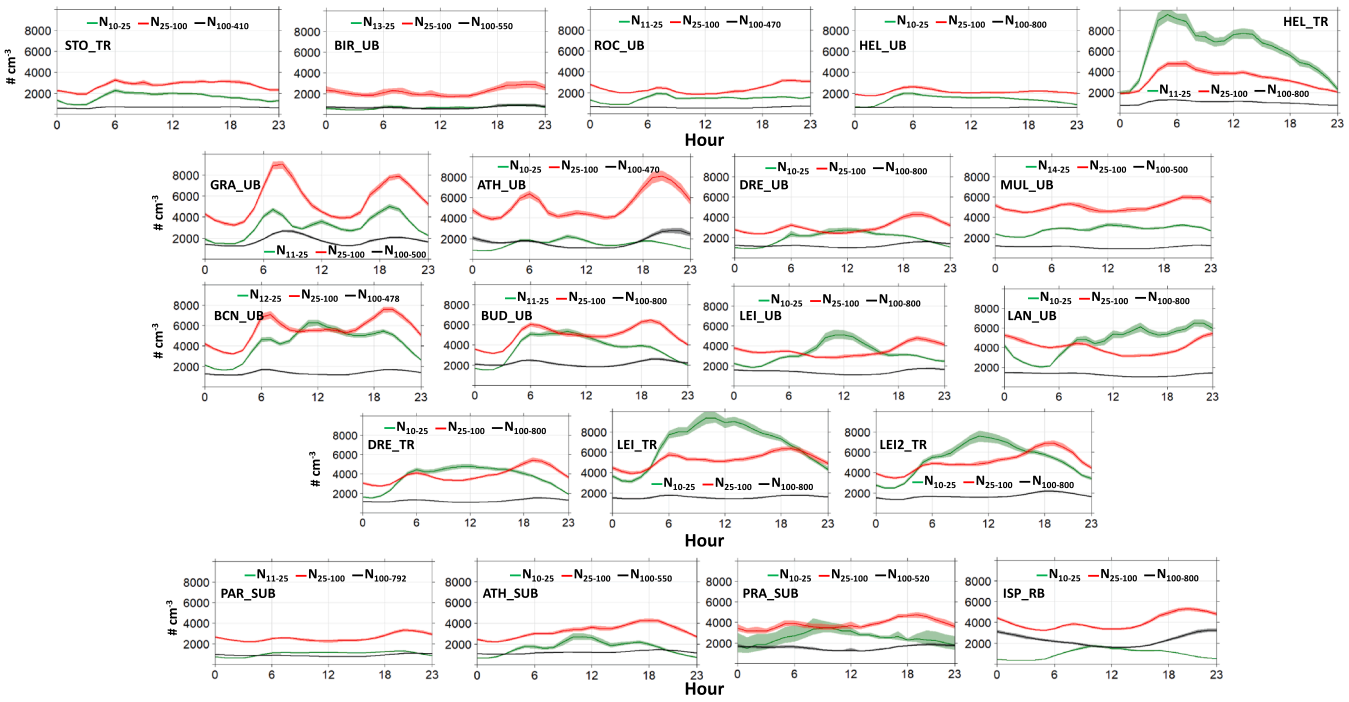

Fig. 5. Averaged 2017–2019 hourly concentrations of the particle number fractions (in # cm^{-3}) $N_{10\text{-}25}$, $N_{25\text{-}100}$ and $N_{100\text{-}800}$. Only sites with a lower size detection limit of 10–14 nm are included. UB, Urban background; TR, Traffic; SUB, Suburban background; RB, Regional background.

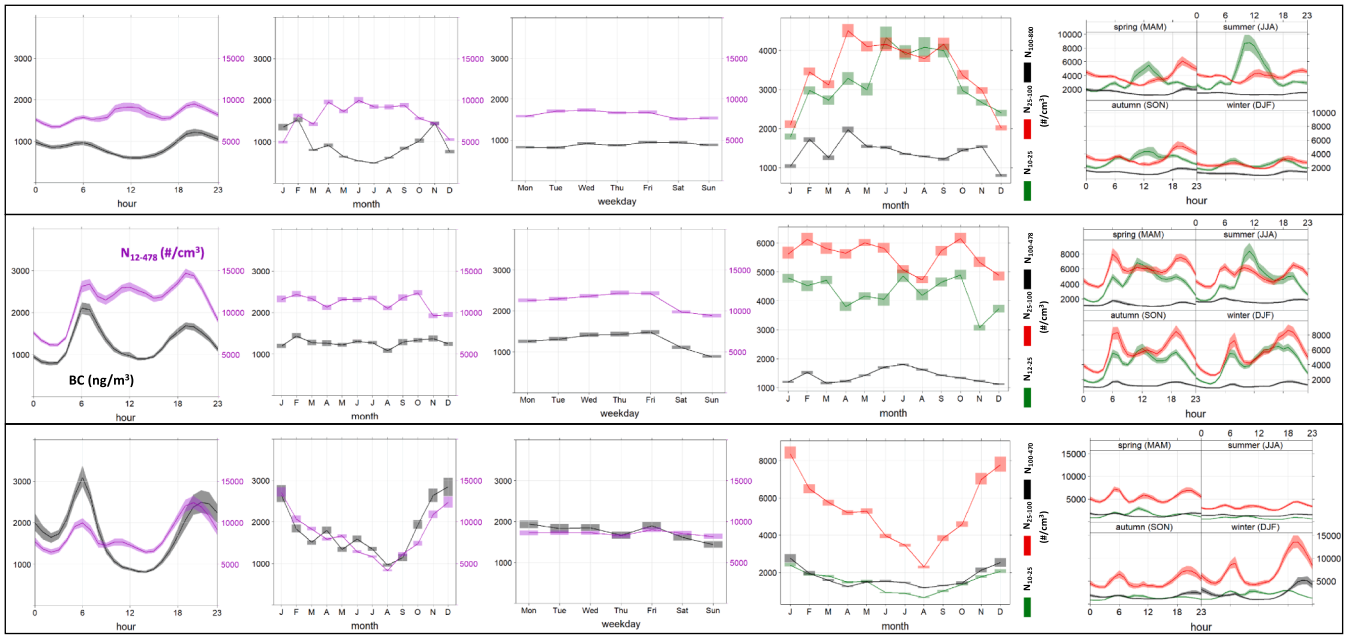

Fig. 6. Daily and seasonal patterns of UFP and BC for three Urban background stations in South Europe: LEI_UB, BCN_UB and ATH_UB.

peak, but no seasonal patterns were noticeable, with similar PNC and BC all year. These sites also had high summer Nucleation mode peaks at midday, with lower intensities in spring and autumn. Weekend BC and PNC were markedly lower. These sites had weak seasonal patterns or no covariation of BC with PNC. However, some of these sites (BIR_UB, MUL_UB, HEL_UB, LIL_SUB, LND_UB, LND2_UB and LND_TR) had greater prevalence of traffic, with weak or no midday peaks and with traffic rush hour peaks. Other stations (ATH_SUB, BUD, DRE_TR and ISP_RB) had greater prevalence of midday peaks, but did not exhibit the typical behaviour of high PNC and low BC values in summer (Table S3).

This categorisation is similar to that proposed by Sun et al. (2019) for numerous sites in Germany.

3.6. Correlation of PNCs with ancillary pollutants and meteorological parameters

3.6.1. Black carbon

Using the twenty-four averaged dataset concentrations supplying PNC and BC data, it was observed that BC concentrations were poorly correlated with $N_{10\text{-}25}$ ($R^2 = 0.14$, Figure S3). However, the correlation was high ($R^2 = 0.81$, Figure S3) for $N_{25\text{-}100}$ as a result of the major traffic contribution to this mode and the absence of the effect of differences in

the lowest size detection limits used. As for BC (Fig. 4), the Aitken mode peaked at traffic rush hours (Fig. 5). This result was expected given that the reported size mode of traffic contributions to ambient urban PNC is around 40 nm. Road traffic is also the main source of BC in European cities producing very high correlations of PNC and BC during traffic rush hours (Rodríguez and Cuevas, 2007; Sun et al., 2019). However, at traffic sites, this peak could also be in the Nucleation mode (Brines et al., 2015; Harrison et al., 2019, 2011; Hopke et al., 2022; Rivas et al., 2020; Wehner et al., 2002). The correlation of BC with $N_{100\text{-}800}$ was also high but lower than for $N_{25\text{-}100}$ ($R^2 = 0.65$, Figure S3), indicating a major traffic origin with partial contributions of other sources, such as regional aerosol transport (among others).

Correlation of BC with PNC ($N_{10\text{-}800}$) and $N_{25\text{-}800}$ was high, with $R^2 = 0.60$ and 0.85, respectively, when including the averages of all sites; $R^2 = 0.26$ and 0.89 for TR sites; $R^2 = 0.71$ and 0.85 for UB sites; and $R^2 = 0.85$ and 0.90 for SUB and RB sites (Figure S4). High correlations between these factors were also found by Sun et al. (2019) for numerous sites in Germany. The high correlation of average BC with $N_{25\text{-}800}$ reflects the impact of traffic pollution on air quality; thus, cities which are highly polluted have higher concentrations of co-pollutants than cleaner cities. However, when considering $N_{10\text{-}800}$ and $N_{10\text{-}25}$ (Figures S3 and S4), the correlation decreased markedly because (i) the Nucleation mode particles have mixed origins (traffic, nucleation, aviation, shipping, fumigation for upper atmospheric layers, and biomass burning, among others) and (ii) the differences in the lower size detection limits are considerable. When correlating BC and PNC individually for each site using hourly data for 2017–2019, high correlation ($R^2 = 0.60$–0.66) was obtained for three sites, and moderate correlation ($R^2 = 0.39$–0.57) for the other ten sites; while for the other eleven sites, the correlation was low ($R^2 = 0.18$ with an exceptionally small value at LEI_UB of $R^2 = 0.01$) (Table S4). When considering $N_{25\text{-}800}$ instead of PNC, the correlation with BC markedly increased in such a way that the correlation was high for six sites ($R^2 = 0.60$–0.78), moderate for another ten sites ($R^2 = 0.40$–0.46) and lower in the remaining eight sites ($R^2 = 0.26$–0.34, with the exception of LEI_UB at $R^2 = 0.05$) (Table S4).

The correlation of $N_{25\text{-}100}$ and $N_{100\text{-}800}$ with BC was high ($R^2 = 0.72$ and 0.62–0.88) for one and nine sites, respectively; and moderate ($R^2 = 0.40$–0.56 and 0.40–0.58) in the other eight and thirteen sites, respectively, of the twenty-four sites that measure UFP and BC (Table S5). For $N_{10\text{-}25}$, the correlation was very low in nineteen out of the twenty-four cases ($R^2 = 0.04$–0.10) and low to moderately low in the other five ($R^2 = 0.16$–0.36) (Table S5).

The above correlation ranges are again similar to those found by Sun et al. (2019) and Wu et al. (2015) in Germany and streets in Edinburgh during different campaigns and at different sites, and it is essential to highlight that:

i. The correlation of BC with the mean $N_{10\text{-}800}$ and $N_{25\text{-}800}$ values of the sites indicates that these equally reflect the impact of road traffic emissions on air quality;
ii. The correlation analysis of individual sites shows that for BC vs. $N_{10\text{-}800}$ 69% of the sites reached moderately-high (39%) and moderately-low (35%) correlations, but for 26% of the sites the correlation was low;
iii. For $N_{25\text{-}800}$ the correlation with BC increased at 96% of the sites (high 70%, moderate 26%);
iv. Adequate monitoring of the Nucleation mode UFPs might supply information very relevant to monitoring the impact of other sources and processes.

However, it is recommended that future studies:

i. Start measurements at sizes even lower than 10 nm by using instruments such as co-located Particle Size Magnifiers (PSM) or Nano-CPCs;
ii. Meet ACTRIS and CEN requirements on size measurements ($N_{10\text{-}800}$).

This will allow harmonised and systematic data compilation for, e.g., aerosol health studies, more detailed process-level studies, and better interpretation of the results.

3.6.2. Other ancillary pollutants and meteorological parameters

As for the other ancillary pollutants, low correlations were found between PNC and CO and SO_2, when considering the 2017–2019 individual averages (Table S6), only for UB sites ($R^2 = 0.21$ for both CO and SO_2). When considering $N_{25\text{-}800}$ rather than PNC, the correlation was the same for CO and slightly higher for SO_2 ($R^2 = 0.21$ and 0.42, respectively); and for CO, a moderately-low correlation ($R^2 = 0.36$) was also found for TR sites. For the individual sites (Table S4), low to moderate correlations with PNC ($R^2 = 0.17$–0.54) were found only for five sites out of the seventeen co-measuring SO_2; but low to moderately-high correlations with PNC ($R^2 = 0.16$–0.65) were found in eleven of the sixteen sites co-measuring CO. For $N_{25\text{-}800}$, the correlation did not increase for the same five sites with low to moderate correlation ($R^2 = 0.13$–0.53) for SO_2 and the same eleven sites with low to moderate-high correlation ($R^2 = 0.13$–0.71) for CO.

For NO and NO_2, moderate-low correlations were obtained with PNC when considering the averaged concentrations (Table S6) of only UB sites ($R^2 = 0.27$ and 0.35, respectively); but these increased for $N_{25\text{-}800}$ at TR ($R^2 = 0.70$ and 0.63 for NO and NO_2, respectively) and UB ($R^2 = 0.35$ and 0.48) sites. For SUB and RB sites, significant moderate-low to moderate-high correlations were attained for PNC and $N_{25\text{-}800}$ with NO ($R^2 = 0.23$ and 0.63). This is because urban NO_x and BC are emitted at a high proportion by diesel vehicles (Degraeuwe et al., 2016; Ježek et al., 2015; Tunno et al., 2018). Furthermore, Harrison and Jones (2005) reported similar correlations between PNC and NO_x at one TR site (Marylebone Rd., with $R^2 = 0.63$) and at several UB sites (Belfast Centre, Glasgow Centre, Birmingham Centre and London Bloomsbury, with $R^2 = 0.37$, 0.39, 0.46 and 0.43, respectively). A higher correlation of both NO and NO_2 with $N_{25\text{-}800}$ was thus expected at TR sites.

When considering the individual datasets (Table S4), low-moderate correlations between PNC with NO_2 and NO ($R^2 = 0.22$ to 0.58, slightly higher for NO_2) were obtained only at TR sites. For the sixteen UB sites co-measuring NO_2 and NO, only twelve and nine, respectively, reached moderate-low to moderate-high correlations ($R^2 = 0.23$ to 0.68 for NO_2 and $R^2 = 0.21$ to 0.54 for NO), while for SUB and RB sites, correlations decreased and varied greatly ($R^2 = 0.07$ to 0.40) for both pollutants. Similar results were obtained for $N_{25\text{-}800}$ with NO_2 and NO, with slightly lower correlations of NO and NO_2 at TR sites ($R^2 = 0.11$ to 0.56), but higher correlations at UB sites: all UB sites had $R^2 = 0.16$–0.69 for NO_2 and twelve out of fourteen UB sites had $R^2 = 0.16$ to 0.56 with NO. Again, for the SUB and RB sites, correlations varied greatly ($R^2 = 0.06$ to 0.44) for both pollutants. Thus, as for BC, the results show that in most UB and TR sites, there was a significant co-hourly variation of NO_2 and NO with PNC and $N_{25\text{-}800}$.

For PNC and PM_{10} (Table S6), the correlation was negative and moderate-low for TR sites ($R^2 = 0.32$) and was positive and moderate-low to moderate-high for UB and SUB + RB sites ($R^2 = 0.37$ and 0.68). For $N_{25\text{-}800}$, the correlation markedly increased for UB and SUB + RB sites ($R^2 = 0.53$ and 0.91) but not for TR sites ($R^2 = 0.00$). For $PM_{2.5}$ and PNC (Table S6), the correlation increased from TR ($R^2 = 0.05$) to UB ($R^2 = 0.40$) and to SUB + RB ($R^2 = 0.77$); and increased when considering $N_{25\text{-}800}$ ($R^2 = 0.77$ TR, 0.49 UB and 0.91 SUB + RB). Thus, when the regions/sites of Europe recorded higher $PM_{2.5}$ concentrations, PNC, especially of $N_{25\text{-}800}$, was also high.

However, the results of evaluations of individual sites (Table S4) differ considerably, -with low PNC- PM_{10} correlations: only eight sites reached $R^2 = 0.16$–0.36 and sixteen reached $R^2 = 0.00$–0.12. For $N_{25\text{-}800}$, the correlation with PM_{10} increased slightly, with twelve sites reaching $R^2 = 0.16$–0.45 and twelve reaching $R^2 = 0.00$–0.14. A similar situation was found for $PM_{2.5}$ and PNC correlations, with only four sites reaching $R^2 = 0.19$–0.34 and thirteen reaching $R^2 = 0.00$–0.14. Again, for $N_{25\text{-}800}$ the correlation increased slightly, with seven sites reaching

R^2 = 0.17–0.47 and ten reaching R^2 = 0.04–0.15. For the different modes, as expected, the correlations of the Nucleation mode concentrations with PM_{10} and $PM_{2.5}$ were significantly lower at all sites (R^2 = 0.00–0.11 and 0.00–0.07, respectively, Table S5). For the Aitken mode, low-moderate correlations were only reached at four sites for PM_{10} (R^2 = 0.20–0.22) and $PM_{2.5}$ (R^2 = 0.16–0.31) and for all other sites, correlations even decreased: R^2 = 0.00–0.14 and 0.01–0.13, respectively (Table S5). The correlation increased for the Accumulation mode with PM_{10}, at R^2 = 0.16–0.64 (R^2 = 0.04–0.15 for the remaining five sites). All seventeen sites measured correlations with $PM_{2.5}$ reaching R^2 = 0.19–0.79 (Table S5). De Jesus et al. (2019) found low correlations of $PM_{2.5}$ and PNC in a global study involving ten cities located in North America, Europe, Asia, and Australia, with r^2 = from 0.01 to 0.48.

Using the averaged concentrations for the different sites, correlations were low for O_3 with PNC and $N_{25\text{-}800}$ (Table S6) for UB and SUB + RB sites ($R^2 < 0.07$), with the exception of $N_{25\text{-}800}$ at SUB + RB sites (R^2 = 0.24). Markedly higher negative PNC and $N_{25\text{-}800}$ O_3 correlations were obtained for TR sites, at R^2 = 0.72 and 0.91, respectively. However, for the individual sites (Table S4), the correlation of PNC and $N_{25\text{-}800}$ with O_3 was low and negative in all cases, with only seven and eight out of twenty-three sites reaching R^2 = 0.19 to 0.39, respectively, and much lower correlations in all the other cases.

When using 2017–2019 average data for meteorological parameters from all sites, a moderate-low to moderate positive correlation was obtained for both PNC and $N_{25\text{-}800}$ with T and insolation (R^2 = 0.28 to 0.53) and a negative correlation with relative humidity (R^2 = 0.27 to 0.46) was obtained for UB sites (Table S6). This result is probably a product of the gradient from the low UFP pollution in N Europe to higher UFP pollution in S and E Europe. When using the single site hourly datasets (Table S4), correlations were found to be low for all parameters evaluated (mostly from negative to positive, R^2 = 0.09), with a more positive trend for Nucleation mode vs. insolation and a more negative trend for wind speed with all PNC size modes, relative humidity, and Nucleation mode particles (Table S5).

4. Conclusions and limitations

This work summarises the first results on ultrafine particle (UFP) particle-size distribution (PNSD) in urban areas of Europe from the RI-URBANS project. This includes 2017–2019 datasets from twenty-seven air quality monitoring sites. The focus is mostly on urban background (UB) and traffic (TR) concentrations, but it also includes four suburban (SUB) and a regional background (RB) sites.

4.1. Measurements

Only fourteen out of twenty-seven datasets reached >70% of data availability, reflecting the complexity of UFP-PNSD measurements, which require detailed monitoring and constant maintenance of the instrumentation. Furthermore, the lack of harmonisation of PNSD measurement accounts for significant differences of the lower size detection limits (3 to 20 nm), which makes the direct comparison of UFP and particle number concentrations (PNC) concentrations from different sites difficult, especially those in the Nucleation mode (<25 nm). To increase comparability, an effort should be made to implement the ACTRIS and CEN recommendations in the near future.

From the twenty-seven datasets, only twelve are openly available in the EBAS data infrastructure, and accordingly, an effort should also directed at making data open for use in air quality health research and policy support, especially if the data is obtained with public funds.

4.2. Levels and PNSD

The results show a clear increasing $N_{10\text{-}800}$ UB concentration trend from Northern to Southern and Eastern Europe, and an even more marked trend for $N_{25\text{-}100}$ and $N_{25\text{-}800}$. These trends are similar to those found for Black Carbon (BC). As it could be expected, PNCs follow the TR > UB > SUB trend. However, PNC in the RB of the Po Valley are equivalent to those of an UB in Southern Europe.

The major contributing source to PNC in urban Europe is road traffic as deduced from the parallel daily patterns to those of BC, with peak concentrations at traffic rush hours. However, a relevant number of sites recorded high PNCs (in some cases exceeding those of traffic) in the morning-midday coinciding with minimal BC, and the highest temperature, wind speed, insolation and O_3. These marked morning-midday maxima are caused by pronounced increases of $N_{10\text{-}25}$ (Nucleation mode).

It is important to note that the highest midday PNC-Nucleation modes are recorded in Central Europe followed by Southern Europe, so they do not follow only insolation as it should be expected from new particle formation from regional photochemical nucleation. Thus, the origin of these midday marked maxima are attributed to: photochemical nucleation, surface fumigation of high-altitude atmospheric layers transporting high SO_2 plumes and plumes from airports, shipping, or power or industrial plants. In a relevant proportion of the study sites, the contribution of these sources/processes to the annual PNC is very significant.

Daily and seasonal patterns are used to classify the PNSD datasets in three major groups: i) low midday PNC peaks and PNC parallel daily patterns, with high winter BC and PNC, with low spring-summer $N_{10\text{-}25}$; ii) PNC and BC traffic-related daily patterns, but a major midday PNC peak with low BC concentrations, with inverse seasonal PNC (highest in spring-summer) and BC (highest in autumn–winter) patterns, with very intensive $N_{10\text{-}25}$ midday peaks in spring and summer); and iii) as type ii, but with dominant traffic-related PNC peaks, but marked midday $N_{10\text{-}25}$ peaks and no definite seasonal patterns.

Strong correlations between averaged BC and PNC concentrations, especially for BC and $N_{25\text{-}800}$, of the different datasets indicate that there is a clear impact of road traffic emissions on air quality in UB environments, with different degree across Europe. However, for the individual datasets BC-PNC are notably lower, because i) there are more sources contributing to PNC than traffic; ii) the high midday PNC in many of the sites decrease BC-PNC correlation. Moderate-correlations are also attained for the individual sites for $N_{25\text{-}800}$ and NO and NO_2 for UB and TR sites.

These findings support the need of measuring PNCs accurately, especially the Nucleation mode, to properly evaluate the occurrence of sources other than traffic contributing to the health effects of UFP. To this end, RI-URBANS strongly recommends starting measurements below 10 nm by using instruments such as co-located Particle Size Magnifiers (PSM) or Nano-CPCs and implementing the above recommended protocols for UFP-PNSD measurements.

Further steps in the study of these datasets will focus on source apportionment analyses and the epidemiological assessments to evaluate short-term associations with PNCs, size modes and source contributions.

4.3. Limitations

As a major limitation we should acknowledge the problems in directly comparing the datasets due to different protocols used for PNSD measurements and quality assurance. Thus, the DRE_UB, LAN_UB, LEI_UB, DRE_TR, LEI and LEI2_TR datasets were obtained following the ACTRIS protocols for measurements of PNSD, and the instruments are frequently undergoing quality assurance exercises by the World Calibration Centre for Aerosol Physics (WCCAP, https://www.eurochamp.org/calibration-centres/wccap). The datasets from ATH_UB, BCN_UB, GRA_UB, HEL_UB, MAD_UB, HEL_TR, ATH_SUB, LIL_SUB, PRA_SUB, ISP_RB are produced by ACTRIS collaborators or partners, and they are obtained with protocols tending to follow the ones from ACTRIS but have not recently or have never undergone the quality checks by the WCCAP. Finally, the datasets of BIR_UB, BUD_UB, LND and LND2_UB,

MAR_UB, ROC_UB, ZUR_UB, PAR_SUB, LND_TR and STO_TR are obtained from highly specialized research teams, but data uncertainty remains unknown. The lack of harmonisation has caused variability in the lower size detection limit leading to large differences in the total number of measured particles. In this study, this discrepancy is reduced by comparing concentrations in the range of 10–800 and 25–800 nm, but there is an urgent need to harmonise measurement protocols such as following ACTRIS and CEN recommendations to provide directly comparable UFP-PNSD datasets.

Credit authorship contribution statement

The corresponding author, Pedro Trechera, is responsible for ensuring that the descriptions are accurate and agreed upon by all authors, and was involved in data collection, treatment and processing. Also, is the responsible to write the manuscript.

Meritxell Garcia-Marlès was involved into data treatment, data processing and writing, including the revision of the manuscript.

Xavier Querol is the coordinator of the project and accordingly, he did conceptualisation, supervision, but also as member of the writing lead team of this paper was involved data treatment, data processing and writing, including the revision of the manuscript.

Xiansheng Liu did the correlation of UFP-PNSD for each individual dataset from 2017-2019 with BC, ancillary pollutants and meteorological parameters.

Roy M. Harrison, Philip K. Hopke, Tuukka Petäjä and Andrés Alastuey provided the 2017-2019 datasets for the different sites, assisted and contributed in the processing of the dataset. In addition, they carried out a thorough proofreading of the manuscript before obtaining the final version of the manuscript.

Cristina Reche, Noemí Pérez, Marjan Savadkoohi, David Beddows, Imre Salma, Máté Vörösmarty, Andrea Casans, Juan Andrés Casquero-Vera, Christoph Hueglin, Nicolas Marchand, Benjamin Chazeau, Grégory Gille, Panayiotis Kalkavouras, Nikos Mihalopoulos, Jakub Ondracek, Nadia Zikova, Jarkko V. Niemi, Hanna E. Manninen, David C. Green, Anja H. Tremper, Michael Norman, Stergios Vratolis, Konstantinos Eleftheriadis, Francisco J. Gómez-Moreno, Elisabeth Alonso-Blanco, Holger Gerwig, Alfred Wiedensohler, Kay Weinhold, Maik Merkel, Susanne Bastian, Jean-Eudes Petit, Olivier Favez, Suzanne crumeyrolle, Nicolas Ferlay, Sebastiao Martins Dos Santos, Jean-Philippe Putaud, Hilkka Timonen, Janne Lampilahti, Christof Asbach, Carmen Wolf, Heinz Kaminski, Hicran Altug, Barbara Hoffmann, David Q. Rich and Marco Pandolfi provided the 2017-2019 datasets for the different sites, assisted and contributed in the processing of the dataset and carefully reviewed the manuscript.

Declaration of Competing Interest

The authors declare that they have no known competing financial interests or personal relationships that could have appeared to influence the work reported in this paper.

Data availability

The authors do not have permission to share the data from all the sites. However, should there be a request for the data, every effort will be made to share it.

Acknowledgments

This study is supported by the RI-URBANS project (Research Infrastructures Services Reinforcing Air Quality Monitoring Capacities in European Urban & Industrial Areas, European Union's Horizon 2020 research and innovation programme, Green Deal, European Commission, under grant agreement No 101036245). The authors would like to thank ACTRIS (The Aerosol, Clouds and Trace Gases Research Infrastructure), especially the EBAS Data Centre, for providing datasets for the study. The authors would like to thank also the support from "Agencia Estatal de Investigación" from the Spanish Ministry of Science and Innovation, and FEDER funds under the projects CAIAC (PID2019-108990RB-I00); and the Generalitat de Catalunya (AGAUR 2021 SGR00447) and the Direcció General de Territori.

This study is partly funded by the National Institute for Health Research (NIHR) Health Protection Research Unit in Environmental Exposures and Health, a partnership between UK Health Security Agency (UKHSA) and Imperial College London. The views expressed are those of the author(s) and not necessarily those of the NIHR, UKHSA, or the Department of Health and Social Care. The work in Rochester, NY was funded by the New York State Energy Research and Development Authority under contracts #59802 and 125993. This research is also partly supported by the Hungarian Research, Development and Innovation Office (grant no. K132254). We thank the Hessian Agency for Nature Conservation, Environment and Geology (HLNUG), Wiesbaden, Germany for providing concentrations of ancillary pollutants of urban background station at Darmstadt. The Stockholm traffic station (Hornsgatan) datasets were provided thanks to the nPETS project (grant agreement no. 954377) funded by the European Union (EU).

Appendix A. Supplementary data

Supplementary data to this article can be found online at https://doi.org/10.1016/j.envint.2023.107744.

References

ACTRIS, C. for A.I.-S.M., Preliminary, 2021. Preliminary ACTRIS recommendation for aerosol in-situ sampling, measurements, and analysis. https://www.actris.eu/sites/default/files/2021-06/Preliminary%20ACTRIS%20recommendations%20for%20aerosol%20in-situ%20measurements%20June%202021.pdf.

Azimi, P., Zhao, D., Stephens, B., 2014. Estimates of HVAC filtration efficiency for fine and ultrafine particles of outdoor origin. Atmos. Environ. 98, 337–346. https://doi.org/10.1016/j.atmosenv.2014.09.007.

Baldauf, R., Devlin, R., Gehr, P., Giannelli, R., Hassett-Sipple, B., Jung, H., Martini, G., McDonald, J., Sacks, J., Walker, K., 2016. Ultrafine Particle Metrics and Research Considerations: Review of the 2015 UFP Workshop. Int. J. Environ. Res. Public Health 13, 1054. https://doi.org/10.3390/ijerph13111054.

Beevers, S.D., Westmoreland, E., de Jong, M.C., Williams, M.L., Carslaw, D.C., 2012. Trends in NO_x and NO_2 emissions from road traffic in Great Britain. Atmos. Environ. 54, 107–116. https://doi.org/10.1016/j.atmosenv.2012.02.028.

Bousiotis, D., Pope, F.D., Beddows, C.S., Dall'Osto, M., Massling, A., Nøjgaard, J.K., Nordstrøm, C., Niemi, J.V., Portin, H., Petäjä, T., Perez, N., Alastuey, A., Querol, X., Kouvarakis, G., Mihalopoulos, N., Vratolis, S., Eleftheriadis, K., Wiedensohler, A., Weinhold, K., Merkel, M., Tuch, T., Harrison, R.M., 2021. A phenomenology of new particle formation (NPF) at 13 European sites. Atmos. Chem. Phys. 21, 11905–11925. https://doi.org/10.5194/acp-21-11905-2021.

Brean, J., Beddows, D.C.S., Shi, Z., Temime-Roussel, B., Marchand, N., Querol, X., Alastuey, A., Minguillon, M.C., Harrison, R.M., 2020. Molecular insights into new particle formation in Barcelona. Spain. Atmos. Chem. Phys. 20, 10029–10045. https://doi.org/10.5194/acp-20-10029-2020.

Brines, M., Dall'Osto, M., Beddows, D.C.S., Harrison, R.M., Gómez-Moreno, F., Núñez, L., Artíñano, B., Costabile, F., Gobbi, G.P., Salimi, F., Morawska, L., Sioutas, C., Querol, X., 2015. Traffic and nucleation events as main sources of ultrafine particles in high-insolation developed world cities. Atmos. Chem. Phys. 15, 5929–5945. https://doi.org/10.5194/acp-15-5929-2015.

Carnerero, C., Pérez, N., Petäjä, T., Laurila, T.M., Ahonen, L.R., Kontkanen, J., Ahn, K.H., Alastuey, A., Querol, X., 2019. Relating high ozone, ultrafine particles, and new particle formation episodes using cluster analysis. Atmos. Environ. X 4, 100051. https://doi.org/10.1016/j.aeaoa.2019.100051.

Carslaw, D.C., Ropkins, K., 2012. openair — An R package for air quality data analysis. Environ. Model. Softw. 27–28, 52–61. https://doi.org/10.1016/j.envsoft.2011.09.008.

Casquero-Vera, J.A., Lyamani, H., Titos, G., Minguillón, M.C., Dada, L., Alastuey, A., Querol, X., Petäjä, T., Olmo, F.J., Alados-Arboledas, L., 2021. Quantifying traffic, biomass burning and secondary source contributions to atmospheric particle number concentrations at urban and suburban sites. Sci. Total Environ. 768, 145282 https://doi.org/10.1016/j.scitotenv.2021.145282.

Cassee F., Morawska L., Peters A. (Eds)., 2019. The White Paper on Ambient Ultrafine Particles: evidence for policy makers. 'Thinking outside the box' Team, October 2019, 23 pp, https://efca.net/files/WHITE%20PAPER-UFP%20evidence%20for%20policy%20makers%20(25%20OCT).pdf.

CEN–TC 264/WG 32 – Air quality - Determination of the particle number concentration [WWW Document], n.d. URL https://standards.iteh.ai/catalog/tc/cen/7c511ec9-b305-4ba0-9447-12098c9050eb/cen-tc-264-wg-32 (accessed 6.20.22).

CEN/–S 16976:2016 – Ambient air - Determination of the particle number concentration of atmospheric aerosol [WWW Document], 2016. URL https://standards.iteh.ai/catalog/standards/cen/91f1ac67-f6d6-408c-af89-e81763194fd3/cen-ts-16976-2016 (accessed 6.20.22).

CEN/–S 17434:2020 – Ambient air - Determination of the particle number size distribution of atmospheric aerosol using a Mobility Particle Size Spectrometer (MPSS) [WWW Document], 2020. URL https://standards.iteh.ai/catalog/standards/cen/a841bc08-ed34-4fa8-94ca-8c5e07b99db9/cen-ts-17434-2020 (accessed 6.20.22).

Cheung, H.C., Morawska, L., Ristovski, Z.D., 2011. Observation of new particle formation in subtropical urban environment. Atmos. Chem. Phys. 11, 3823–3833. https://doi.org/10.5194/acp-11-3823-2011.

Dall'Osto, M., Querol, X., Alastuey, A., O'Dowd, C., Harrison, R.M., Wenger, J., Gómez-Moreno, F.J., 2013. On the spatial distribution and evolution of ultrafine particles in Barcelona. Atmos. Chem. Phys. 13, 741–759. https://doi.org/10.5194/acp-13-741-2013.

Degraeuwe, B., Thunis, P., Clappier, A., Weiss, M., Lefebvre, W., Janssen, S., Vranckx, S., 2016. Impact of passenger car NOx emissions and NO2 fractions on urban NO2 pollution - Scenario analysis for the city of Antwerp. Belgium. Atmos. Environ. 126, 218–224. https://doi.org/10.1016/j.atmosenv.2015.11.042.

Diesch, J.M., Drewnick, F., Klimach, T., Borrmann, S., 2013. Investigation of gaseous and particulate emissions from various marine vessel types measured on the banks of the Elbe in Northern Germany. Atmos. Chem. Phys. 13, 3603–3618. https://doi.org/10.5194/acp-13-3603-2013.

Donaldson, K., Tran, C.L., 2002. Inflammation caused by particles and fibers. Inhal. Toxicol. 14, 5–27. https://doi.org/10.1080/089583701753338613.

EEA, 2021. Europe's air quality status 2021- update, European Environment Agency. https://www.eea.europa.eu/publications/air-quality-in-europe-2021/air-quality-status-briefing-2021.

Eleftheriadis, K., Gini, M.I., Diapouli, E., Vratolis, S., Vasilatou, V., Fetfatzis, P., Manousakas, M.I., 2021. Aerosol microphysics and chemistry reveal the COVID19 lockdown impact on urban air quality. Sci Rep. 11, 14477. https://doi.org/10.1038/s41598-021-93650-6.

Fazli, T., Zeng, Y., Stephens, B., 2019. Fine and ultrafine particle removal efficiency of new residential HVAC filters. Indoor Air 29, ina.12566. https://doi.org/10.1111/ina.12566.

Flagan, R.C., 1998. History of Electrical Aerosol Measurements. Aerosol Sci. Technol. 28, 301–380. https://doi.org/10.1080/02786829808965530.

Gani, S., Chambliss, S.E., Messier, K.P., Lunden, M.M., Apte, J.S., 2021. Spatiotemporal profiles of ultrafine particles differ from other traffic-related air pollutants: Lessons from long-term measurements at fixed sites and mobile monitoring. Environ. Sci. Atmos. 1, 558–568. https://doi.org/10.1039/d1ea00058f.

Grundström, M., Hak, C., Chen, D., Hallquist, M., Pleijel, H., 2015. Variation and co-variation of PM_{10}, particle number concentration, NO_x and NO_2 in the urban air – Relationships with wind speed, vertical temperature gradient and weather type. Atmos. Environ. 120, 317–327. https://doi.org/10.1016/j.atmosenv.2015.08.057.

Harrison, R.M., Beddows, D.C.S., Alam, M.S., Singh, A., Brean, J., Xu, R., Kotthaus, S., Grimmond, S., 2019. Interpretation of particle number size distributions measured across an urban area during the FASTER campaign. Atmos. Chem. Phys. 19, 39–55. https://doi.org/10.5194/acp-19-39-2019.

Harrison, R.M., Beddows, D.C.S., Dall'Osto, M.,, 2011. PMF analysis of wide-range particle size spectra collected on a major highway. Environ. Sci. Technol. 45, 5522–5528. https://doi.org/10.1021/es2006622.

Harrison, R.M., Jones, A.M., 2005. Multisite Study of Particle Number Concentrations in Urban Air. Environ. Sci. Technol. 39, 6063–6070. https://doi.org/10.1021/es040541e.

Hofman, J., Staelens, J., Cordell, R., Stroobants, C., Zikova, N., Hama, S.M.L., Wyche, K. P., Kos, G.P.A., Van Der Zee, S., Smallbone, K.L., Weijers, E.P., Monks, P.S., Roekens, E., 2016. Ultrafine particles in four European urban environments: Results from a new continuous long-term monitoring network. Atmos. Environ. 136, 68–81. https://doi.org/10.1016/j.atmosenv.2016.04.010.

Hopke, P.K., Feng, Y., Dai, Q., 2022. Source apportionment of particle number concentrations: A global review. Sci. Total Environ. 819, 153104 https://doi.org/10.1016/j.scitotenv.2022.153104.

ISO, 2015. ISO/TS–80004-2:2015 - Nanotechnologies — Vocabulary — Part 2: Nano-objects [WWW Document], 2015. URL https://www.iso.org/standard/54440.html (accessed 6.20.22).

de Jesus, A.L., Rahman, M.M., Mazaheri, M., Thompson, H., Knibbs, L.D., Jeong, C., Evans, G., Nei, W., Ding, A., Qiao, L., Li, L., Portin, H., Niemi, J.V., Timonen, H., Luoma, K., Petäjä, T., Kulmala, M., Kowalski, M., Peters, A., Cyrys, J., Ferrero, L., Manigrasso, M., Avino, P., Buonano, G., Reche, C., Querol, X., Beddows, D., Harrison, R.M., Sowlat, M.H., Sioutas, C., Morawska, L., 2019. Ultrafine particles and PM2.5 in the air of cities around the world: Are they representative of each other? Environ. Int. 129, 118–135. https://doi.org/10.1016/j.envint.2019.05.021.

Ježek, I., Katrašnik, T., Westerdahl, D., Močnik, G., 2015. Black carbon, particle number concentration and nitrogen oxide emission factors of random in-use vehicles measured with the on-road chasing method. Atmos. Chem. Phys. 15, 11011–11026. https://doi.org/10.5194/acp-15-11011-2015.

Joerger, V.M., Pryor, S.C., 2018. Ultrafine particle number concentrations and size distributions around an elevated highway viaduct. Atmos. Poll. Res. 9, 714–722. https://doi.org/10.1016/j.apr.2018.01.008.

Johansson, C., Norman, M., Gidhagen, L., 2007. Spatial & temporal variations of PM_{10} and particle number concentrations in urban air. Environ. Monit. Assess. 127, 477–487. https://doi.org/10.1007/s10661-006-9296-4.

Junkermann, W., Vogel, B., Bangert, M., 2016. Ultrafine particles over Germany – an aerial survey. Tellus B Chem. Phys. Meteorol. 68, 29250. https://doi.org/10.3402/tellusb.v68.29250.

Kalkavouras, P., Bougiatioti, A., Hussein, T., Kalivitis, N., Stavroulas, I., Michalopoulos, P., Mihalopoulos, N., 2021. Regional new particle formation over the eastern mediterranean and middle east. Atmosphere (Basel). 12, 1–23. https://doi.org/10.3390/atmos12010013.

Kangasluoma, J., Cai, R., Jiang, J., Deng, C., Stolzenburg, D., Ahonen, L.R., Chan, T., Fu, Y., Kim, C., Laurila, T.M., Zhou, Y., Dada, L., Sulo, J., Flagan, R.C., Kulmala, M., Petäjä, T., Lehtipalo, K., 2020. Overview of measurements and current instrumentation for 1–10 nm aerosol particle number size distributions. J. Aerosol Sci. 148, 105584 https://doi.org/10.1016/j.jaerosci.2020.105584.

Kelly, F.J., Fussell, J.C., 2012. Size, source and chemical composition as determinants of toxicity attributable to ambient particulate matter. Atmos. Environ. 60, 504–526. https://doi.org/10.1016/j.atmosenv.2012.06.039.

Kerminen, V.-M., Chen, X., Vakkari, V., Petäjä, T., Kulmala, M., Bianchi, F., 2018. Atmospheric new particle formation and growth: review of field observations. Environ. Res. Lett. 13, 103003 https://doi.org/10.1088/1748-9326/aadf3c.

Knibbs, L.D., Cole-Hunter, T., Morawska, L., 2011. A review of commuter exposure to ultrafine particles and its health effects. Atmos. Environ. 45, 2611–2622. https://doi.org/10.1016/j.atmosenv.2011.02.065.

Kreyling, W.G., Semmler, M., Erbe, F., Mayer, P., Takenaka, S., Schulz, H., Oberdörster, G., Ziesenis, A., 2002. Translocation of ultrafine insoluble iridium particles from lung epithelium to extrapulmonary organs is size dependent but very low. J. Toxicol. E–viron. Heal. - Part A. 65, 1513–1530. https://doi.org/10.1080/00984100290071649.

Kulmala, M., Petäjä, T., Ehn, M., Thornton, J., Sipilä, M., Worsnop, D.R., Kerminen, V.-M., 2014. Chemistry of atmospheric nucleation: On the recent advances on precursor characterization and atmospheric cluster composition in connection with atmospheric new particle formation. Annu. Rev. Phys. Chem. 65, 21–37. https://doi.org/10.1146/annurev-physchem-040412-110014.

Kumar, P., Morawska, L., Birmili, W., Paasonen, P., Hu, M., Kulmala, M., Harrison, R.M., Norford, L., Britter, R., 2014. Ultrafine particles in cities. Environ. Int. https://doi.org/10.1016/j.envint.2014.01.013.

Lehtipalo, K., Ahonen, L.R., Baalbaki, R., Sulo, J., Chan, T., Laurila, T., Dada, L., Duplissy, J., Miettinen, E., Vanhanen, J., Kangasluoma, J., Kulmala, M., Petäjä, T., Jokinen, T., 2022. The standard operating procedure for Airmodus Particle Size Magnifier and nano-condensation Nucleus Counter. J. Aerosol. Sci. 159, 105896 https://doi.org/10.1016/j.jaerosci.2021.105896.

Lorentz, H., Janicke, U., Jakobs, H., Schmidt, W., Hellebrandt, P., Ketzel, M., Gerwig, H., 2019. Ultrafine particle dispersion modelling at and around Frankfurt airport (FRA), Germany. 19th International Conference on Harmonisation within Atmospheric Dispersion Modelling for Regulatory Purposes. 3-6 June 2019, Bruges, Belgium, H19-082. https://www.harmo.org/Conferences/Proceedings/_Bruges/publishedSections/H19-082%20Helmut%20Lorentz.pdf.

Maher, B.A., Ahmed, I.A.M., Karloukovski, V., MacLaren, D.A., Foulds, P.G., Allsop, D., Mann, D.M.A., Torres-Jardón, R., Calderon-Garciduenas, L., 2016. Magnetite pollution nanoparticles in the human brain. P. Natl. Acad. Sci. USA 113, 10797–10801. https://doi.org/10.1073/pnas.1605941113.

Manninen, H.E., Mirme, S., Mirme, A., Petäjä, T., Kulmala, M., 2016. How to reliably detect molecular clusters and nucleation mode particles with Neutral cluster and Air Ion Spectrometer (NAIS). Atmos. Meas. Technol. 9, 3577–3605. https://doi.org/10.5194/amt-9-3577-2016.

Montagne, D.R., Hoek, G., Klompmaker, J.O., Wang, M., Meliefste, K., Brunekreef, B., 2015. Land Use Regression Models for Ultrafine Particles and Black Carbon Based on Short-Term Monitoring Predict Past Spatial Variation. Environ. Sci. Tech. 49 (14), 8712–8720. https://doi.org/10.1021/es505791g.

Morelli, X., Foraster, M., Aguilera, I., Basagana, X., Corradi, E., Deltell, A., Ducret-Stich, R., Phuleria, H., Ragettli, M.S., Rivera, M., Thomasson, A., Künzli, N., Slama, R., 2015. Short-term associations between traffic-related noise, particle number and traffic flow in three European cities. Atmos. Environ. 103, 25–33. https://doi.org/10.1016/j.atmosenv.2014.12.012.

Németh, Z., Salma, I., 2014. Spatial extension of nucleating air masses in the Carpathian Basin. Atmos. Chem. Phys. 14, 8841–8848. https://doi.org/10.5194/acp-14-8841-2014.

Nguyen, C., Soulhac, L., Salizzoni, P., 2018. Source Apportionment and Data Assimilation in Urban Air Quality Modelling for NO2: The Lyon Case Study. Atmosphere (Basel). 9, 8. https://doi.org/10.3390/atmos9010008.

Oberdörster, G., Oberdörster, E., Oberdörster, J., 2005. Nanotoxicology: an emerging discipline evolving from studies of ultrafine particles. Environ. Health Perspect. 113, 823–839. https://doi.org/10.1289/ehp.7339.

Oberdörster, G., Sharp, Z., Atudorei, V., Elder, A., Gelein, R., Kreyling, W., Cox, C., 2004. Translocation of inhaled ultrafine particles to the brain. Inhal. Toxicol. 16, 437–445. https://doi.org/10.1080/08958370490439597.

Okuljar, M., Kuuluvainen, H., Kontkanen, J., Garmash, O., Olin, M., Niemi, J.V., Timonen, H., Kangasluoma, J., Tham, Y.J., Baalbaki, R., Sipilä, M., Salo, L., Lintusaari, H., Portin, H., Teinilä, K., Aurela, M., Dal Maso, M., Rönkkö, T., Petäjä, T., Paasonen, P., 2021. Measurement report: The influence of traffic and new particle formation on the size distribution of 1–800 nm particles in Helsinki: a street canyon and an urban background station comparison. Atmos. Chem. Phys. 21, 9931–9953. https://doi.org/10.5194/acp-21-9931-2021.

Petäjä, T., Kerminen, V.-M., Dal Maso, M., Junninen, H., Koponen, I.K., Hussein, T., Aalto, P.P., Andronopoulos, S., Robin, D., Hämeri, K., Bartzis, J.G., Kulmala, M., 2007. Sub-micron atmospheric aerosols in the surroundings of Marseille and Athens: physical characterization and new particle formation. Atmos. Chem. Phys. 7, 2705–2720. https://doi.org/10.5194/acp-7-2705-2007, 2007.

Peters, A., Veronesi, B., Calderón-Garcidueñas, L., Gehr, P., Chen, L.C., Geiser, M., Reed, W., Rothen-Rutishauser, B., Schürch, S., Schulz, H., 2006. Translocation and potential neurological effects of fine and ultrafine particles a critical update. Part. Fibre Toxicol. 3, 13. https://doi.org/10.1186/1743-8977-3-13.

Petzold, A., Hasselbach, J., Lauer, P., Baumann, R., Franke, K., Gurk, C., Schlager, H., Weingartner, E., 2008. Experimental studies on particle emissions from cruising ship, their characteristic properties, transformation and atmospheric lifetime in the marine boundary layer. Atmos. Chem. Phys. 8, 2387–2403. https://doi.org/10.5194/acp-8-2387-2008.

Putaud, J.-P., Pozzoli, L., Pisoni, E., Martins Dos Santos, S., Lagler, F., Lanzani, G., Dal Santo, U., Colette, A., 2021. Impacts of the COVID-19 lockdown on air pollution at regional and urban background sites in northern Italy. Atmos. Chem. Phys. 21, 7597–7609. https://doi.org/10.5194/acp-21-7597-2021.

Qi, X.M., Ding, A.J., Nie, W., Petäjä, T., Kerminen, V.-M., Herrmann, E., Xie, Y.N., Zheng, L.F., Manninen, H., Aalto, P., Sun, J.N., Xu, Z.N., Chi, X.G., Huang, X., Boy, M., Virkkula, A., Yang, X.-Q., Fu, C.B., Kulmala, M., 2015. Aerosol size distribution and new particle formation in western Yangtze River Delta of China: two-year measurement at the SORPES station. Atmos. Chem. Phys. 15, 12445–12464. https://doi.org/10.1039/D1EA00096A.

Querol, X., Massagué, J., Alastuey, A., Moreno, T., Gangoiti, G., Mantilla, E., Duéguez, J. J., Escudero, M., Monfort, E., Pérez García-Pando, C., Petetin, H., Jorba, O., Vázquez, V., de la Rosa, J., Campos, A., Muñóz, M., Monge, S., Hervás, M., Javato, R., Cornide, M.J., 2021. Lessons from the COVID-19 air pollution decrease in Spain: Now what? Sci. Total Environ. 779, 146380 https://doi.org/10.1016/j.scitotenv.2021.146380.

Reche, C., Querol, X., Alastuey, A., Viana, M., Pey, J., Moreno, T., Rodríguez, S., González, Y., Fernández-Camacho, R., De La Campa, A.M.S., De La Rosa, J., Dall'Osto, M., Prévt, A.S.H., Hueglin, C., Harrison, R.M., Quincey, P., 2011. New considerations for PM, Black Carbon and particle number concentration for air quality monitoring across different European cities. Atmos. Chem. Phys. 11, 6207–6227. https://doi.org/10.5194/acp-11-6207-2011.

Rivas, I., Beddows, D.C.S., Amato, F., Green, D.C., Järvi, L., Hueglin, C., Reche, C., Timonen, H., Fuller, G.W., Niemi, J.V., Pérez, N., Aurela, M., Hopke, P.K., Alastuey, A., Kulmala, M., Harrison, R.M., Querol, X., Kelly, F.J., 2020. Source apportionment of particle number size distribution in urban background and traffic stations in four European cities. Environ. Int. 135, 105345 https://doi.org/10.1016/j.envint.2019.105345.

Rivas, I., Vicens, L., Basagaña, X., Tobías, A., Katsouyanni, K., Walton, H., Hüglin, C., Alastuey, A., Kulmala, M., Harrison, R.M., Pekkanen, J., Querol, X., Sunyer, J., Kelly, F.J., 2021. Associations between sources of particle number and mortality in four European cities. Environ. Int. 155 https://doi.org/10.1016/j.envint.2021.106662.

Rodríguez, S., Cuevas, E., 2007. The contributions of "minimum primary emissions" and "new particle formation enhancements" to the particle number concentration in urban air. J. Aerosol Sci. 38, 1207–1219. https://doi.org/10.1016/j.jaerosci.2007.09.001.

Rönkkö, T., Kuuluvainen, H., Karjalainen, P., Keskinen, J., Hillamo, R., Niemi, J.V., Pirjola, L., Timonen, H.J., Saarikoski, S., Saukko, E., Järvinen, A., Silvennoinen, H., Rostedt, A., Olin, M., Yli-Ojanperä, J., Nousiainen, P., Kousa, A., Dal Maso, M., 2017. Traffic is a major source of atmospheric nanocluster aerosol. Proc. Natl. Acad. Sci. U. S. A. 114, 7549–7554. https://doi.org/10.1073/pnas.1700830114.

Salma, I., Borsós, T., Weidinger, T., Aalto, P., Hussein, T., Dal Maso, M., Kulmala, M., 2011. Production, growth and properties of ultrafine atmospheric aerosol particles in an urban environment. Atmos. Chem. Phys. 11, 1339–1353. https://doi.org/10.5194/acp-11-1339-2011.

Salma, I., Füri, P., Németh, Z., Balásházy, I., Hofmann, W., Farkas, Á., 2015. Lung burden and deposition distribution of inhaled atmospheric urban ultrafine particles as the first step in their health risk assessment. Atmos. Environ. 104, 39–49. https://doi.org/10.1016/j.atmosenv.2014.12.060.

Salma, I., Vörösmarty, M., Gyöngyösi, A.Z., Thén, W., Weidinger, T., 2020. What can we learn about urban air quality with regard to the first outbreak of the COVID-19 pandemic? A case study from central Europe. Atmos. Chem. Phys. 20, 15725–15742. https://doi.org/10.5194/acp-20-15725-2020.

Sánchez Jiménez, A., Heal, M.R., Beverland, I.J., 2012. Correlations of particle number concentrations and metals with nitrogen oxides and other traffic-related air pollutants in Glasgow and London. Atmos. Environ. 54, 667–678. https://doi.org/10.1016/j.atmosenv.2012.01.047.

Sandrini, S., Fuzzi, S., Piazzalunga, A., Prati, P., Bonasoni, P., Cavalli, F., Bove, M.C., Calvello, M., Cappelletti, D., Colombi, C., Contini, D., de Gennaro, G., Di Gilio, A., Fermo, P., Ferrero, L., Gianelle, V., Giugliano, M., Ielpo, P., Lonati, G., Marinoni, A., Massabò, D., Molteni, U., Moroni, B., Pavese, G., Perrino, C., Perrone, M.G., Perrone, M.R., Putaud, J.P., Sargolini, T., Vecchi, R., Gilardoni, S., 2014. Spatial and seasonal variability of carbonaceous aerosol across Italy. Atmos. Environ. 99, 587–598. https://doi.org/10.1016/j.atmosenv.2014.10.032.

Stacey, B., Harrison, R.M., Pope, F.D., 2021. Evaluation of aircraft emissions at London Heathrow Airport. Atmos. Environ. 254, 118226 https://doi.org/10.1016/j.atmosenv.2021.118226.

Stanier, C.O., Khlystov, A.Y., Pandis, S.N., 2004. Nucleation events during the Pittsburgh Air Quality Study: Description and relation to key meteorological, gas phase, and aerosol parameters. Aerosol Sci. Technol. 38, 253–264. https://doi.org/10.1080/02786820390229570.

Sun, J., Birmili, W., Hermann, M., Tuch, T., Weinhold, K., Spindler, G., Schladitz, A., Bastian, S., Löschau, G., Cyrys, J., Gu, J., Flentje, H., Briel, B., Asbach, C., Kaminski, H., Ries, L., Sohmer, R., Gerwig, H., Wirtz, K., Meinhardt, F., Schwerin, A., Bath, O., Ma, N., Wiedensohler, A., 2019. Variability of black carbon mass concentrations, sub-micrometer particle number concentrations and size distributions: results of the German Ultrafine Aerosol Network ranging from city street to High Alpine locations. Atmos. Environ. 202, 256–268. https://doi.org/10.1016/j.atmosenv.2018.12.029.

Thén, W., Salma, I., 2022. Particle Number Concentration: A Case Study for Air Quality Monitoring. Atmos. 13, 570. https://doi.org/10.3390/atmos13040570.

Thomson, E.S., Weber, D., Bingemer, H.G., Tuomi, J., Ebert, M., Pettersson, J.B.C., 2018. Intensification of ice nucleation observed in ocean ship emissions. Sci. Rep. 8, 1–9. https://doi.org/10.1038/s41598-018-19297-y.

Tobías, A., Rivas, I., Reche, C., Alastuey, A., Rodríguez, S., Fernández-Camacho, R., Sánchez de la Campa, A.M., de la Rosa, J., Sunyer, J., Querol, X., 2018. Short-term effects of ultrafine particles on daily mortality by primary vehicle exhaust versus secondary origin in three Spanish cities. Environ. Int. 111, 144–151. https://doi.org/10.1016/j.envint.2017.11.015.

Torkmahalleh, M.A., Akhmetvaliyeva, Z., Omran, A.D., Darvish Omran, F., Kazemitabar, M., Naseri, M., Naseri, M., Sharifi, H., Malekipirbazari, M., Kwasi Adotey, E., Gorjinezhad, S., Eghtesadi, N., Sabanov, S., Alastuey, A., de Fátima Andrade, M., Buonanno, G., Carbone, S., Cárdenas-Fuentes, D.E., Cassee, F.R., Dai, Q., Henríquez, A., Hopke, P.K., Keronen, P., Khwaja, H.A., Kim, J., Kulmala, M., Kumar, P., Kushta, J., Kuula, J., Massagué, J., Mitchell, T., Mooibroek, D., Morawska, L., Niemi, J.V., Ngagine, S.H., Norman, M., Oyama, B., Oyola, P., Öztürk, F., Petäjä, T., Querol, X., Rashidi, Y., Reyes, F., Ross-Jones, M., Salthammer, T., Savvides, C., Stabile, L., Sjöberg, K., Söderlund, K., Sunder Raman, R., Timonen, H., Umezawa, M., Viana, M., Xie, S., 2021. Global Air Quality and COVID-19 Pandemic: Do We Breathe Cleaner Air? Aerosol Air Qual. Res. 21, 200567 https://doi.org/10.4209/aaqr.200567.

Tunno, B.J., Tripathy, S., Kinnee, E., Michanowicz, D.R., Shmool, J.L., Cambal, L., Chubb, L., Roper, C., Clougherty, J.E., 2018. Fine-Scale Source Apportionment Including Diesel-Related Elemental and Organic Constituents of $PM_{2.5}$ across Downtown Pittsburgh. Int. J. Environ. Res. Public Health. 15, 2177. https://doi.org/10.3390/ijerph15102177.

Valavanidis, A., Fiotakis, K., Vlachogianni, T., 2008. Airborne particulate matter and human health: Toxicological assessment and importance of size and composition of particles for oxidative damage and carcinogenic mechanisms. J. Enviro–. Sci. Heal. - Part C Environ. Carcinog. Ecotoxicol. Rev. 26, 339–362. https://doi.org/10.1080/10590500802494538.

Wehner, B., Birmili, W., Gnauk, T., Wiedensohler, A., 2002. Particle number size distributions in a street canyon and their transformation into the urban-air background: Measurements and a simple model study. Atmos. Environ. 36, 2215–2223. https://doi.org/10.1016/S1352-2310(02)00174-7.

Von Bismarck-Osten, C., Birmili, W., Ketzel, M., Massling, A., Petäjä, T., Weber, S., 2013. Characterization of parameters influencing the spatio-temporal variability of urban particle number size distributions in four European cities. Atmos. Environ. 77, 415–429. https://doi.org/10.1016/j.atmosenv.2013.05.029.

Vratolis, S., Gini, M.I., Bezantakos, S., Stavroulas, I., Kalivitis, N., Kostenidou, E., Louvaris, E., Siakavaras, D., Biskos, G., Mihalopoulos, N., Pandis, S.N., Pilinis, C., Papayannis, A., Eleftheriadis, K., 2019. Particle number size distribution statistics at City-Centre Urban Background, urban background, and remote stations in Greece during summer. Atmos. Environ. 213, 11–726. https://doi.org/10.1016/j.atmosenv.2019.05.064.

Weichenthal, S., Mallach, G., Kulka, R., Black, A., Wheeler, A., You, H., St-Jean, M., Kwiatkowski, R., Sharp, D., 2013. A randomized double-blind crossover study of indoor air filtration and acute changes in cardiorespiratory health in a First Nations community. Indoor Air 23, 175–184. https://doi.org/10.1111/ina.12019.

WHO, 2021a. Ambient (outdoor) air pollution. 22 September 2021, https://www.who.int/news-room/fact-sheets/detail/ambient-(outdoor)-air-quality-and-health.

WHO, 2021b. WHO global air quality guidelines: particulate matter (PM2.5 and PM10), ozone, nitrogen dioxide, sulfur dioxide and carbon monoxide. World Health Organization. 273 pp, https://apps.who.int/iris/handle/10665/345329.

WHO, 2016. Ambient air pollution: a global assessment of exposure and burden of disease. World Health Organization., 121 pp, https://apps.who.int/iris/handle/10665/250141.

WHO, 2013. Review of evidence on health aspects of air pollution – REVIHAAP Project Technical Report. https://doi.org/10.1007/BF00379640.

Wiedensohler, A., Birmili, W., Nowak, A., Sonntag, A., Weinhold, K., Merkel, M., Wehner, B., Tuch, T., Pfeifer, S., Fiebig, M., Fjäraa, A.M., Asmi, E., Sellegri, K., Depuy, R., Venzac, H., Villani, P., Laj, P., Aalto, P., Ogren, J.A., Swietlicki, E., Williams, P., Roldin, P., Quincey, P., Hüglin, C., Fierz-Schmidhauser, R., Gysel, M., Weingartner, E., Riccobono, F., Santos, S., Grüning, C., Faloon, K., Beddows, D., Harrison, R., Monahan, C., Jennings, S.G., O'Dowd, C.D., Marinoni, A., Horn, H.G., Keck, L., Jiang, J., Scheckman, J., McMurry, P.H., Deng, Z., Zhao, C.S., Moerman, M., Henzing, B., De Leeuw, G., Löschau, G., Bastian, S., 2012. Mobility particle size spectrometers: Harmonization of technical standards and data structure to facilitate high quality long-term observations of atmospheric particle number size distributions. Atmos. Meas. Tech. 5, 657–685. https://doi.org/10.5194/amt-5-657-2012.

Wiedensohler, A., Wiesner, A., Weinhold, K., Birmili, W., Hermann, M., Merkel, M., Müller, T., Pfeifer, S., Schmidt, A., Tuch, T., Velarde, F., Quincey, P., Seeger, S., Nowak, A., 2018. Mobility particle size spectrometers: Calibration procedures and measurement uncertainties. Aerosol Sci. Technol. 52, 146–164. https://doi.org/10.1080/02786826.2017.1387229.

Wolf, K., Cyrys, J., Harcinícková, T., Gu, J., Kusch, T., Hampel, R., Schneider, A., Peters, A., 2017. Land use regression modeling of ultrafine particles, ozone, nitrogen oxides and markers of particulate matter pollution in Augsburg. Germany. Sci. Total Environ. 579, 1531–1540. https://doi.org/10.1016/j.scitotenv.2016.11.160.

Wu, H., Reis, S., Lin, C., Beverland, I.J., Heal, M.R., 2015. Identifying drivers for the intra-urban spatial variability of airborne particulate matter components and their

interrelationships. Atmos. Environ. 112, 306–316. https://doi.org/10.1016/j.atmosenv.2015.04.059.

Yao, L., Garmash, O., Bianchi, F., Zheng, J., Yan, C., Kontkanen, J., Junninen, H., Mazon, S.B., Ehn, M., Paasonen, P., Sipilä, M., Wang, M., Wang, X., Xiao, S., Chen, H., Lu, Y., Zhang, B., Wang, D., Fu, Q., Geng, F., Li, L., Wang, H., Qiao, L., Yang, X., Chen, J., Kerminen, V.M., Petäjä, T., Worsnop, D.R., Kulmala, M., Wang, L., 2018. Atmospheric new particle formation from sulfuric acid and amines in a Chinese megacity. Science 80 (361), 278–281. https://doi.org/10.1126/science.aao4839.

Zhu, Y., Hinds, W.C., Kim, S., Sioutas, C., 2002a. Concentration and size distribution of ultrafine particles near a major highway. J. Air Waste Manage. Assoc. 52, 1032–1042. https://doi.org/10.1080/10473289.2002.10470842.

Zhu, Y., Hinds, W.C., Kim, S., Shen, S., Sioutas, C., 2002b. Study of Ultrafine Particles Near a Major Highway with Heavy-Duty Diesel Traffic. Atmos. Environ. 36, 4323–4335. https://doi.org/10.1016/S1352-2310(02)00354-0.